Cancer Cell

Article

Therapeutic targeting of EP300/CBP by bromodomain inhibition in hematologic malignancies

Graphical abstract

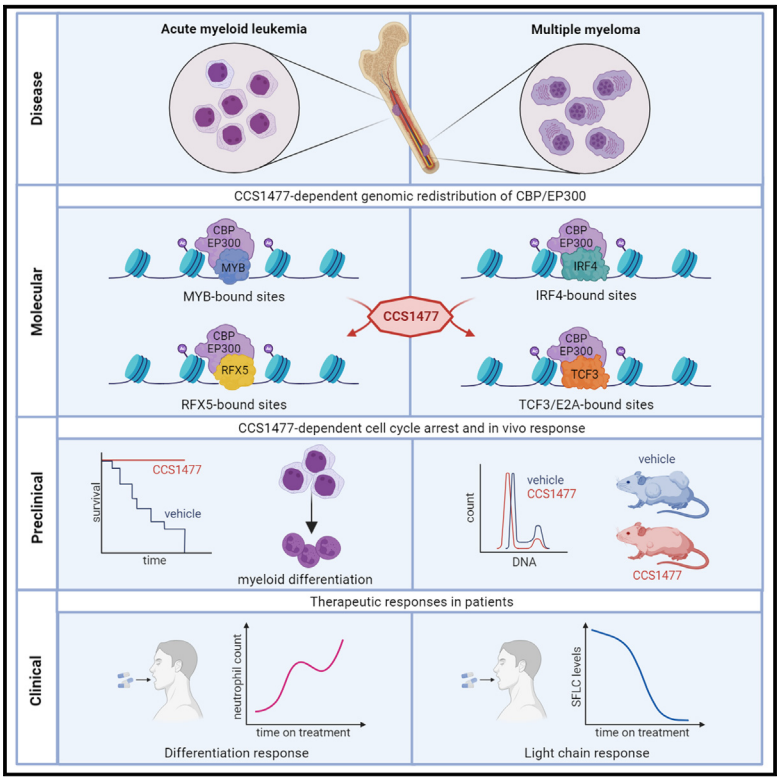

Highlights

- EP300/CBP bromodomain inhibitor CCS1477 is active in hematologic malignancy
- CCS1477 redistributes EP300/CBP from MYB- to RFX-bound enhancers in AML
- CCS1477 redistributes EP300/CBP from IRF4- to E2A-bound enhancers in myeloma
- In phase 1, CCS1477 induces differentiation and objective responses in AML and myeloma

Authors

Luciano Nicosia, Gary J. Spencer, Nigel Brooks, ..., Mhairi Copland, Emma Searle, Tim C.P. Somervaille

Correspondence

tim.somervaille@cruk.manchester.ac.uk

In brief

Nicosia et al. find that CCS1477 (inobrodib), an EP300/CBP bromodomain inhibitor, induces cell-cycle arrest and differentiation in hematologic malignancy models through disrupting EP300/CBP recruitment to enhancer networks occupied by critical transcription factors. In patients with relapsed/refractory disease, CCS1477 monotherapy induces differentiation responses in AML and objective responses in myeloma.

Nicosia et al., 2023, Cancer Cell *41*, 2136–2153
December 11, 2023
https://doi.org/10.1016/j.ccell.2023.11.001

CellPress

CellPress
OPEN ACCESS

Cancer Cell

Article

Therapeutic targeting of EP300/CBP by bromodomain inhibition in hematologic malignancies

Luciano Nicosia,[1,7] Gary J. Spencer,[1,7] Nigel Brooks,[2,7] Fabio M.R. Amaral,[1] Naseer J. Basma,[1] John A. Chadwick,[1] Bradley Revell,[1] Bettina Wingelhofer,[1] Alba Maiques-Diaz,[1] Oliver Sinclair,[1] Francesco Camera,[1] Filippo Ciceri,[1] Daniel H. Wiseman,[3] Neil Pegg,[2] Will West,[2] Tomasz Knurowski,[2] Kris Frese,[2] Karen Clegg,[2] Victoria L. Campbell,[4] James Cavet,[5] Mhairi Copland,[6] Emma Searle,[5] and Tim C.P. Somervaille[1,5,8,*]

[1]Leukaemia Biology Laboratory, Cancer Research UK Manchester Institute, The University of Manchester, Manchester M20 4BX, UK
[2]CellCentric Ltd., Cambridge CB10 1XL, UK
[3]Epigenetics of Haematopoiesis Group, The University of Manchester, Manchester M20 4BX, UK
[4]Western General Hospital, Edinburgh EH4 2XU, UK
[5]The Christie NHS Foundation Trust, Manchester M20 4BX, UK
[6]Paul O'Gorman Leukaemia Research Centre, University of Glasgow, Glasgow G12 0YN, UK
[7]These authors contributed equally
[8]Lead contact
*Correspondence: tim.somervaille@cruk.manchester.ac.uk
https://doi.org/10.1016/j.ccell.2023.11.001

SUMMARY

CCS1477 (inobrodib) is a potent, selective EP300/CBP bromodomain inhibitor which induces cell-cycle arrest and differentiation in hematologic malignancy model systems. In myeloid leukemia cells, it promotes rapid eviction of EP300/CBP from an enhancer subset marked by strong MYB occupancy and high H3K27 acetylation, with downregulation of the subordinate oncogenic network and redistribution to sites close to differentiation genes. In myeloma cells, CCS1477 induces eviction of EP300/CBP from *FGFR3*, the target of the common (4; 14) translocation, with redistribution away from IRF4-occupied sites to TCF3/E2A-occupied sites. In a subset of patients with relapsed or refractory disease, CCS1477 monotherapy induces differentiation responses in AML and objective responses in heavily pre-treated multiple myeloma. *In vivo* preclinical combination studies reveal synergistic responses to treatment with standard-of-care agents. Thus, CCS1477 exhibits encouraging preclinical and early-phase clinical activity by disrupting recruitment of EP300/CBP to enhancer networks occupied by critical transcription factors.

INTRODUCTION

EP300 and *CREBBP* are paralogous genes coding for multi-domain acetyltransferases targeting diverse proteins.[1–3] EP300/CBP is an attractive therapeutic target in cancer due to its roles in promoting growth and transformation. Its activity is increased by chromosomal translocation in acute myeloid leukemia (AML) (e.g., *MLL-EP300* or *MOZ-CBP*) and point mutations in the inhibitory RING domain.[2,4] While other mutations in EP300/CBP are frequent (e.g., in skin squamous cell carcinoma or lymphoid malignancies), most reduce rather than increase activity, in keeping with a role for EP300/CBP as a tumor suppressor. Intriguingly, however, CBP mutant lymphoma cells exhibit enhanced sensitivity to EP300/CBP inhibitors by comparison with wild-type counterparts.[5] Thus, EP300/CBP inhibition may be effective not just in tumors where EP300/CBP is highly expressed, but also where EP300/CBP mutation enhances dependency on residual alleles.

Development of clinical-grade acetyltransferase inhibitors has been challenging but targeting the EP300/CBP bromodomain has been more fruitful:[6] CCS1477 (inobrodib) is a highly selective EP300/CBP bromodomain inhibitor initially evaluated in castration-resistant prostate cancer.[7] Evidence that EP300/CBP bromodomain inhibition might be effective in hematologic malignancy comes from tool compound and domain-focused CRISPR screening preclinical studies in AML or multiple myeloma.[8–10] We therefore set out to evaluate the activity of CCS1477 in hematologic malignancy.

RESULTS

In vitro sensitivity of diverse hematologic cell line and primary samples to CCS1477

We evaluated the response of human hematologic malignancy cell lines to treatment with CCS1477, a drug which was highly selective for EP300/CBP bromodomains versus all others evaluated in BROMOscan analyses (Table S1). We observed that a wide range of AML, acute lymphoblastic leukemia, non-Hodgkin lymphoma, and multiple myeloma cell lines, including OPM-2 cells resistant to lenalidomide, exhibited dose-dependent growth inhibition in liquid and/or semisolid culture conditions (Figures 1A and S1A–S1C). For selected AML lines, we evaluated

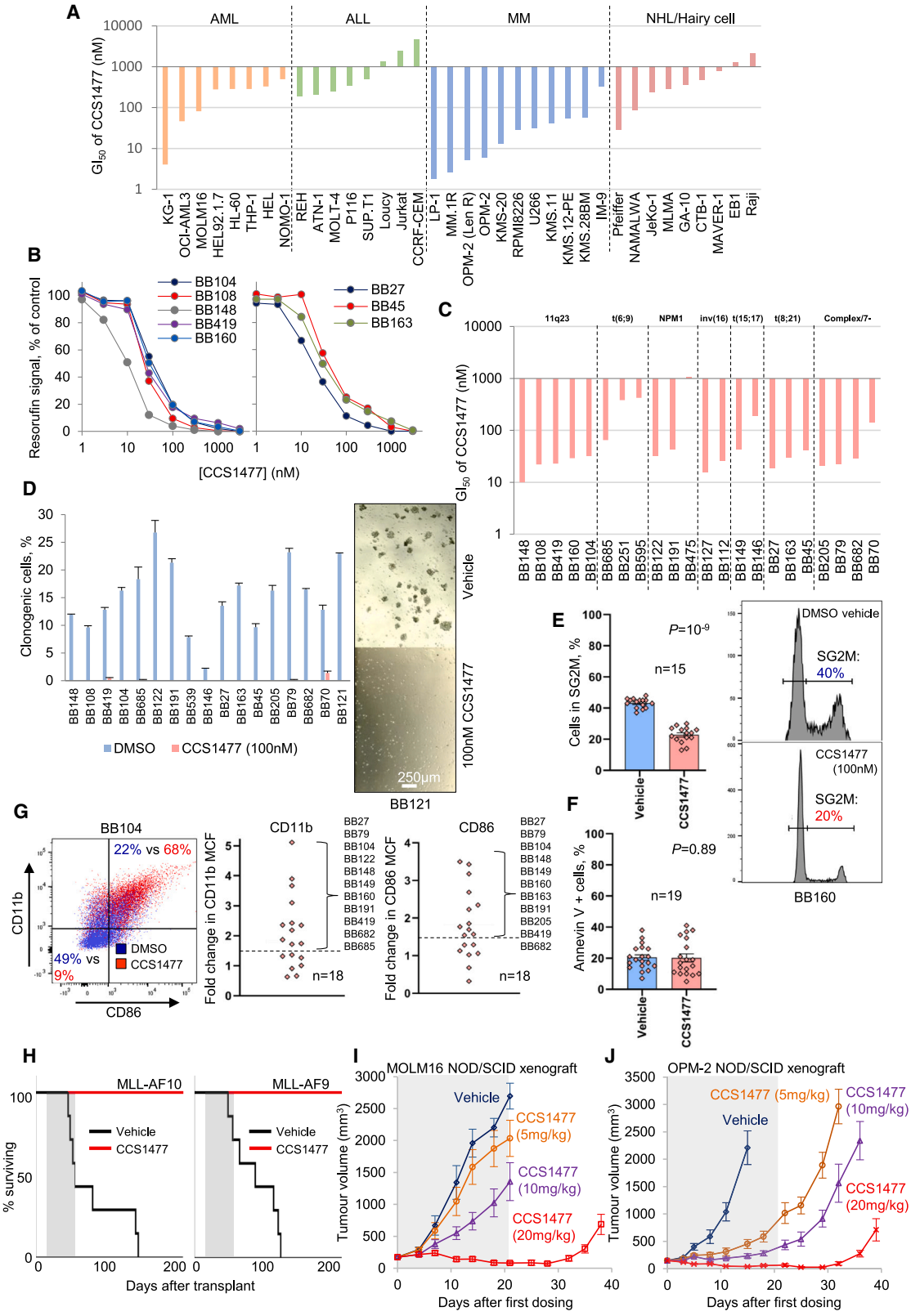

Figure 1. Sensitivity of hematologic malignancy cell lines, primary samples, and mouse models to CCS1477

(A) CellTiter-Glo GI_{50} values for cell lines exposed in duplicate to nine-point dosing of CCS1477 for 120 h. AML, acute myeloid leukemia; ALL, acute lymphoblastic leukemia; MM, multiple myeloma; NHL, non-Hodgkin lymphoma; Len R, cells resistant to lenalidomide.

(legend continued on next page)

cell cycle, differentiation, and apoptosis and noted that growth inhibition was due to cell-cycle arrest with upregulation of cell surface differentiation markers, and only modest levels of apoptosis (Figures S1D–S1F). Similar findings were noted in both human myeloma (Figure S1G) and murine AML cell lines (Figures S1H–S1K).

To extend the evaluation, we performed experiments with primary AML samples and observed that across a wide range of molecular subtypes there was again dose-dependent growth inhibition in liquid and/or semisolid culture conditions (Figures 1B–1D; Table S2) due to cell-cycle arrest (Figure 1E) without increased apoptosis (Figure 1F). Importantly, 72% (13/18) of evaluated AML samples upregulated expression of differentiation-associated cell surface markers (CD11b and/or CD86) by more than 1.5-fold, including those with MLL translocations (BB104, BB148, BB160, BB419), complex karyotype (BB79, BB205, BB682), t(6; 9) (BB685), an NPM1 mutation (BB122, BB191), t(8; 21) (BB27, BB163), and t(15; 17) (BB149) (Figure 1G).

In vivo sensitivity of AML and myeloma murine models to CCS1477

We next evaluated CCS1477 in murine models of AML and myeloma. In a syngeneic model of human *MLL*-translocated AML, we performed secondary transplantation of 10^6 AML cells into sublethally irradiated C57BL/6 mice. Two weeks later, mice were treated with 30 mg/kg CCS1477 daily by oral gavage for 42 days. All mice receiving CCS1477, whether the leukemia was initiated by MLL-AF9 or MLL-AF10, survived to experiment termination on day 220. In contrast, all mice treated with vehicle died of short latency AML (Figures 1H and S2A–S2D). CCS1477 did not induce weight loss in treated mice (Figure S2E). In subcutaneous xenograft models, there was dose-dependent growth inhibition of both MOLM16 AML and OPM-2 myeloma tumors with the highest dose inducing tumor regression and no tumor regrowth until 14 days following CCS1477 withdrawal (Figures 1I and 1J). We assessed the effect of CCS1477 on normal hematopoiesis in Crl:WI(Han) rats and observed thrombocytopenia but no change in hemoglobin or white cells over a two-week treatment at a dose level which modestly impaired weight gain of the treated cohort (Figures S2F and S2G).

These data demonstrate that CCS1477 induces dose-dependent growth inhibition due to cell-cycle arrest across a range of AML and myeloma model systems, with induction of differentiation in AML samples.

Rapid but selective eviction of EP300 from enhancers after CCS1477 treatment of AML cells

To explore the molecular correlates of cellular phenotypes, we initially focused on AML and assessed EP300 genome-wide distribution using chromatin immunoprecipitation with next-generation sequencing (ChIP-seq) in the absence or presence of CCS1477 in THP1 AML cells. THP1 cells respond to drug treatment with cell-cycle arrest and differentiation (Figure S1). As expected, consistent with roles at enhancer elements, EP300 peaks in both steady state and drug-treated cells were predominantly distributed at intronic and intergenic sites (Figures 2A and S3A). In steady state, MEME-ChIP[11] revealed the four strongest centrally enriched transcription factor binding motif clusters under strong EP300-binding peaks to be those for ETS, bZIP, MYB/SANT, and Runt factor classes (Figure 2B). Transcription factors SPI1, CEBPA, MYB, and RUNX1 are respective exemplar members of these classes with high expression in THP1 cells (Table S3).

Next, we compared EP300 ChIP signal in drug versus vehicle-treated cells at multiple time points and identified sites of substantial differential EP300 occupancy. Such sites were defined as those with both an absolute change in ChIP signal (±300 bps from peak summit) of $\geq$25 RPKM (reads per kilobase per million mapped reads) and a fold change in ChIP signal of $\geq$1.25. This allowed categorization of EP300 sites at each time point into those with relative loss of EP300 ChIP signal ("EP300 ↓" sites), those with gain in EP300 ChIP signal ("EP300 ↑" sites) and those with lower or no change in EP300 ChIP signal ("EP300 ↔" sites). Over the 48 h time course, we observed an evolving pattern of change which began within 1 h (Figure 2C): over the first 2 h, there was loss of EP300 ChIP signal at <2% of EP300-binding sites whereas by 48 h there was a mixed pattern of loss and gain, again limited to a subset (<10%) of EP300-occupied sites.

By comparison with strong EP300-binding peaks in steady state (Figure 2B), relative to the enrichment for motifs of other factors there was stronger enrichment for MYB motifs under "EP300 ↓" sites at each time point (Figures 2D and S3B). This prompted us to assess MYB levels by western blot and ChIP-seq. MYB is a critical transcription factor in hematopoiesis with essential functions in normal and leukemic blood cell proliferation and differentiation.[12] Over the first 2 h, there was no reduction in MYB protein (Figures 2E and S3C). At 6 h (Figure 2E), there was a significant although transient reduction in MYB protein, restored to baseline by 24 h (Figure 2F). In contrast, protein levels of SPI1, CEBPA, RUNX1, and EP300 were unchanged (Figures 2E and S3C). ChIP-seq gave similar results; in particular, after both one and 2 h, at "EP300 ↓" sites, there was no concomitant loss of MYB ChIP signal (Figures 2A, 2G, and 2H) whereas at 6 h, consistent with transient reduction in MYB protein levels by western blot, at "EP300 ↓" sites there was both reduced EP300 and reduced MYB ChIP signal (Figures 2I and 2J). Reflecting this evolving pattern of change in EP300 occupancy, there was

(B) Representative dose-response curves of primary AML cells (left panel, *MLL*-rearranged; right panel, t(8; 21) cases; quintuplicate alamarBlue assay after seven days). BB, Biobank identifier.
(C) alamarBlue GI_{50} values, primary AML samples.
(D) Mean + SD clonogenic frequencies of primary human AML cells (triplicate in semisolid culture, 10 days); right panel, representative images. Mean + SEM percentage primary AML cells (E) in SG_2M (n = 15) or (F) annexin V^+ (n = 19) after four days in stromal coculture with vehicle or 100 nM CCS1477; right panel in (E), representative cell cycle profiles (paired t test).
(G) Graphs show fold change in mean cell fluorescence (MCF) for CD11b (middle panel) and CD86 (right panel) for n = 18 primary AML samples after four days in stromal coculture with vehicle or 100 nM CCS1477. Left panel, exemplar flow cytometry plot. Samples with >2-fold increase in MCF are indicated.
(H) Survival curves (n = 7 mice/cohort). Gray boxes indicate CCS1477 treatment. Growth curves show mean + SEM tumor volume for (I) MOLM16 AML and (J) OPM-2 myeloma (n = 5 mice/cohort). Gray boxes indicate CCS1477 treatment. See also Figures S1 and S2, Tables S1 and S2.

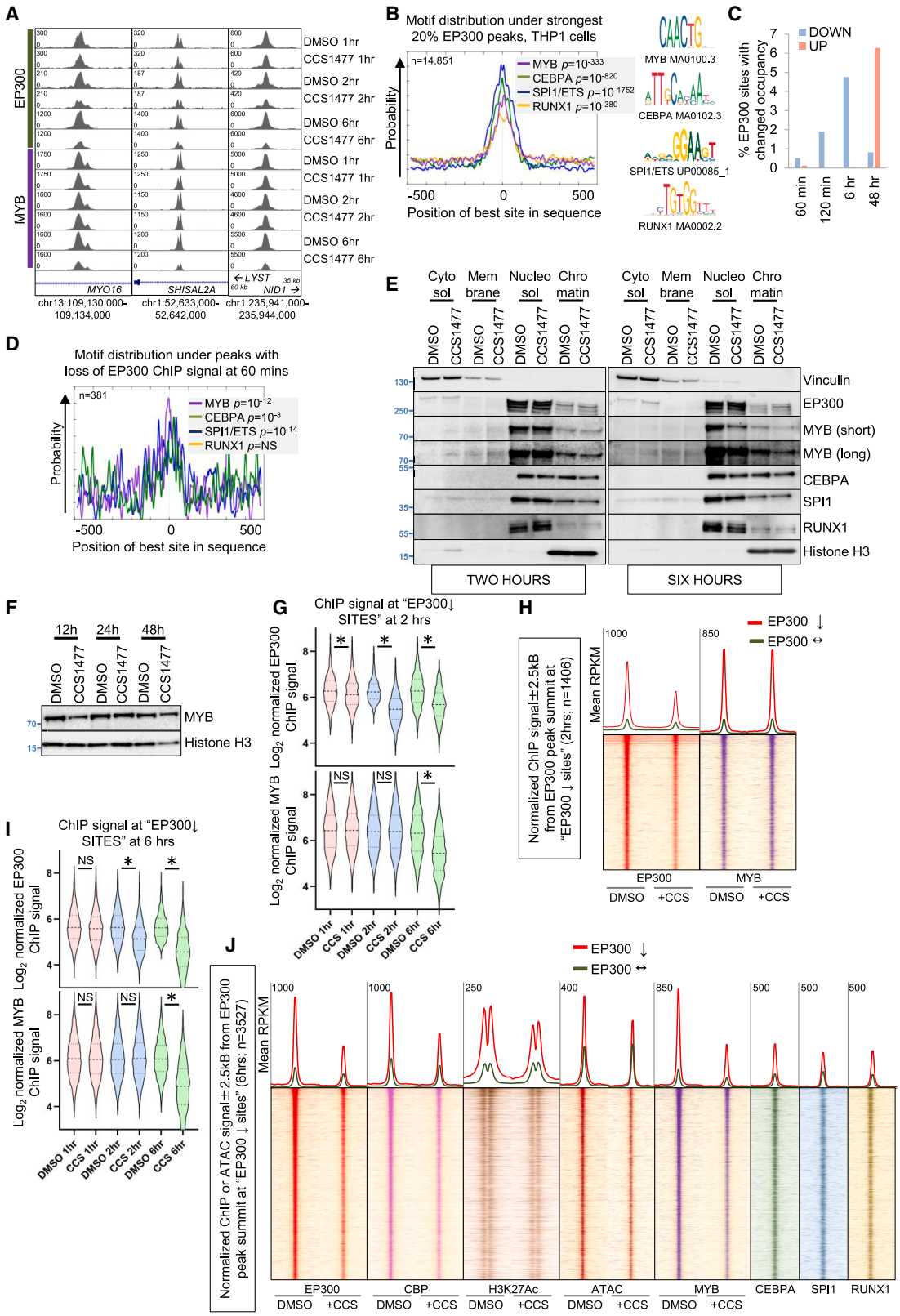

Figure 2. CCS1477 induces rapid but selective loss of EP300 from enhancers in THP1 AML cells

(A) Exemplar ChIP-seq tracks.

(B) Transcription factor motifs under apices of strongest 20% EP300-binding peaks, with MEME-ChIP *E*-values.

(legend continued on next page)

already significant reduction in EP300 ChIP signal at the 1406 "EP300 ↓" sites identified at 2 h when ChIP signal at the same sites was considered at the 1h time point; and likewise, subsequently at 6 h (Figure 2G). Further, at the 3527 "EP300 ↓" sites identified at 6 h, there was already significant reduction of EP300 ChIP signal 2 h following addition of CCS1477 (Figure 2I).

To further characterize EP300-occupied sites disrupted by treatment of cells with CCS1477, and to link to transcription factor occupancy, histone acetylation, and chromatin accessibility, we performed concomitant assay for transposase-accessible chromatin with sequencing (ATAC-seq) and ChIP-seq for CEBPA, CBP, and H3K27Ac, and made use of our prior datasets for SPI1 ChIP-seq in THP1 cells,[13] and RUNX1 in Fujioka AML cells[14] (Figure 2J). The violin plots (Figure 3A) demonstrate that shortly after exposure of cells to CCS1477, EP300 is in particular lost from sites with among the highest levels of EP300, CBP, and MYB occupancy, chromatin accessibility, and surrounding H3K27 acetylation. By comparison with signal observed at the strongest 20% of EP300-binding sites found genome-wide, there was significantly more ChIP signal for MYB, EP300, CBP, and H3K27Ac at "EP300 ↓" sites identified at 1 and 2 h (Figure 3A). This was further emphasized by consideration of the highest confidence "EP300 ↓" sites (i.e., those identified as EP300 ↓ at both one and 2 h; n = 125). Notably, these early "EP300 ↓" sites did not display increased CEBPA or SPI1 ChIP signal by comparison with signal observed at the strongest 20% of EP300-binding sites- (Figure 3A). This at least suggests the possibility that CCS1477 destabilizes recruitment of EP300/CBP at MYB-dominated sites where there is a relative paucity of recruitment of other transcription factors.

6 h following addition of CCS1477, at "EP300 ↓" sites there was also reduced occupancy of CBP, reduced ATAC-seq signal, and reduced surrounding histone acetylation (Figure 2J). Indeed, fold change in ChIP signal for EP300 correlated strongly genome-wide with fold change in CBP (Figure S3D) and H3K27Ac (Figure S3E) ChIP signals, as well as fold change in ATAC-seq signal (Figure S3F), while western blotting showed no change in global H3K27 acetylation and other histone acetylation marks over 48 h (Figure S3G). Strength of ChIP-seq signal for CBP and EP300 at baseline also correlated strongly genome-wide (Figure S3H) indicating that EP300 and CBP occupy the same sites on chromatin with similar strength and are lost from the same subset of genomic regions after addition of CCS1477.

At 48 h, with MYB protein levels returned to baseline (Figures 2F and S4A), a genome-wide redistribution of EP300 binding was evident (Figures 3B and 3C). At "EP300 ↓" sites identified at 48 h, as with earlier time points, there was stronger enrichment for MYB motifs (Figure S3B) by comparison with motifs under the strongest 20% of EP300-binding peaks in steady state (Figure 2B) and stronger MYB occupancy (Figure 3A). Once more, fold change in EP300 ChIP signal correlated strongly with change in chromatin accessibility (Figures 3C and S4B).

At 4,659 "EP300 ↑" sites identified at 48 h there was, in particular, strong enrichment for RFX5 motifs (Figures 3D and 3E), as well as once more for motifs representative of ETS, bZIP, MYB/SANT, and Runt factor classes, although ChIP signal for MYB, RUNX1, CEBPA, and SPI1 was either lower or no different from that observed at "EP300 ↓" sites (Figure 3A). Both ATAC-seq signal and ChIP signal for H3K27Ac at "EP300 ↑" sites were significantly higher than that observed at the strongest 20% of EP300-binding peaks in steady state, at least suggesting the possibility that that the redistribution of EP300/CBP was to sites primed for activation (Figure 3A). Making use of ENCODE ChIP-seq data for RFX5 in the erythroblastic leukemia line K562,[15] we observed that some sites to which EP300 was recruited in THP1 cells were occupied by RFX5 in K562 cells (Figure 3E). RFX5 is a transcription factor known to regulate myeloid differentiation genes.[16] Expression of RFX5, RUNX1, and ETS factor proteins such as FLI1, ELF1, and ETV6 was unaffected by treatment of cells with 100 nM CCS1477 over 48 h (Figures S4C and S4D). Of note, in additional ChIP-seq experiments where THP1 cells were treated with 1000 nM CCS1477, the pattern of EP300 redistribution at both 6 and 48 h was similar to that observed for cells treated with 100 nM (Figure S4E) indicating a dose-level plateau at least as far as redistribution of EP300-binding sites is concerned, and further enhancing confidence in the specificity of CCS1477 for the EP300/CBP bromodomains.

Reflecting the significance of the transcription factor MYB in AML, *MYB* knockdown (KD)—as with CCS1477 treatment—also induced cell-cycle arrest, differentiation, and minimal apoptosis (Figures S4F–S4I). Further, ChIP PCR confirmed eviction of EP300 from a selection of profiled MYB-occupied sites (Figures S4J) and genome-wide there was a strong correlation between baseline MYB occupancy and loss of surrounding H2K27Ac ChIP signal (Figures S4K and S4L) following *MYB* KD.

In summary, within 1 to 2 h, CCS1477 induced eviction of EP300 from a subset of sites in THP1 AML cells marked by strong MYB, EP300, and CBP occupancy, high chromatin accessibility, and strong surrounding H3K27 acetylation; and downstream there evolved over time a widespread redistribution of EP300 occupancy away from sites occupied by MYB and toward those occupied by RFX5, and other factors.

CCS1477-induced eviction of EP300/CBP disables an oncogenic enhancer network

Next, we explored the transcriptional consequences of 100 nM CCS1477 treatment on THP1 cells. At 6 h, and considering 7,299 expressed protein-coding genes (i.e., those with expression levels of 0.5 fragments per kilobase per million mapped reads (FPKM) in at least one of the four bulk RNA sequencing (RNA-seq) samples), 842 were differentially expressed: 227

(C) Graph shows percentage EP300-binding sites with change in EP300 occupancy after 100 nM CCS1477 by time.
(D) MEME-ChIP motif enrichment plot for "EP300 ↓" sites at 1 h. Western blots from THP1 AML cells treated with 100 nM CCS1477 following (E) cellular subfractionation and (F) prolonged treatment with drug. Violin plots show distribution, median (thick dotted line) and interquartile range (light dotted lines) of "EP300 ↓ sites" after (G) 2 and (I) 6 h of 100 nM CCS1477 in indicated conditions. Statistical significance (t test) is denoted by * ($p < 0.01$); NS, not significant. Heatmaps show ATAC or ChIP signal ±2.5 kB from the summit of "EP300 ↓" peaks after (H) 2 and (J) 6 h of 100 nM CCS1477 for indicated factors in indicated conditions. Graphs above heatmaps show mean ChIP signal for the indicated peak group. See also Figures S3 and S4.

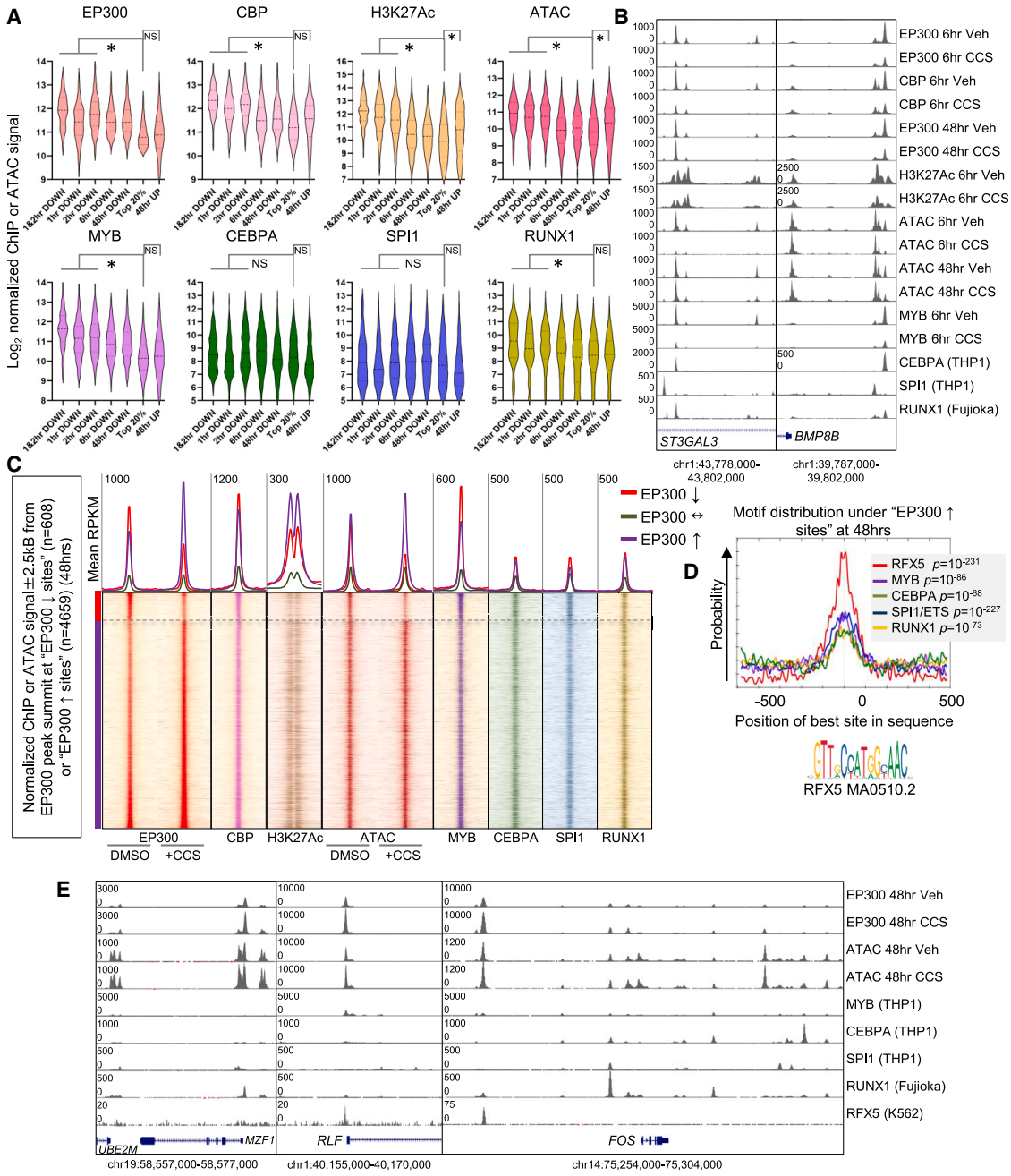

Figure 3. Redistribution of EP300-binding sites upon extended CCS1477 exposure in THP1 AML cells

(A) Violin plots show distribution, median (thick dotted line) and interquartile range (light dotted lines) of ChIP signal for indicated proteins or ATAC signal at indicated genomic regions in THP1 AML cells. Statistical significance is by one-way ANOVA, Tukey post hoc test (* indicates both $p < 0.01$ and >1.2 mean fold change in ChIP signal; NS, not significant).

(B) Exemplar ChIP-seq and ATAC-seq tracks.

(C) Heatmaps show ATAC or ChIP signal ±2.5 kB from summit of EP300-binding peaks in THP1 cells treated for 48 h with 100 nM CCS1477 for indicated factors in indicated conditions. EP300-binding sites are grouped in ranked order of loss ("EP300 ↓" sites) or gain ("EP300 ↑" sites) of EP300 ChIP signal from sites after 48 h of 100 nM CCS1477 treatment. Graphs above heatmaps show mean ChIP signal for indicated peak group.

(D) MEME-ChIP motif enrichment plot for "EP300 ↑" sites at 48 h CCS1477 (100 nM) treatment. (E) Exemplar ChIP-seq and ATAC-seq tracks. See also Figure S4.

genes were upregulated and 615 downregulated (Figure 4A; Table S3; 1.66-fold change in mean expression). Gene ontology (GO) analysis[17] revealed significant enrichment of genes with biological process terms "inflammatory response" ($p = 10^{-12}$), "signal transduction" ($p = 10^{-8}$), "phagocytosis" ($p = 10^{-7}$), and "positive regulation of transcription from RNA polymerase II promoter" ($p = 10^{-6}$) among downregulated genes. There were no significantly enriched terms among upregulated

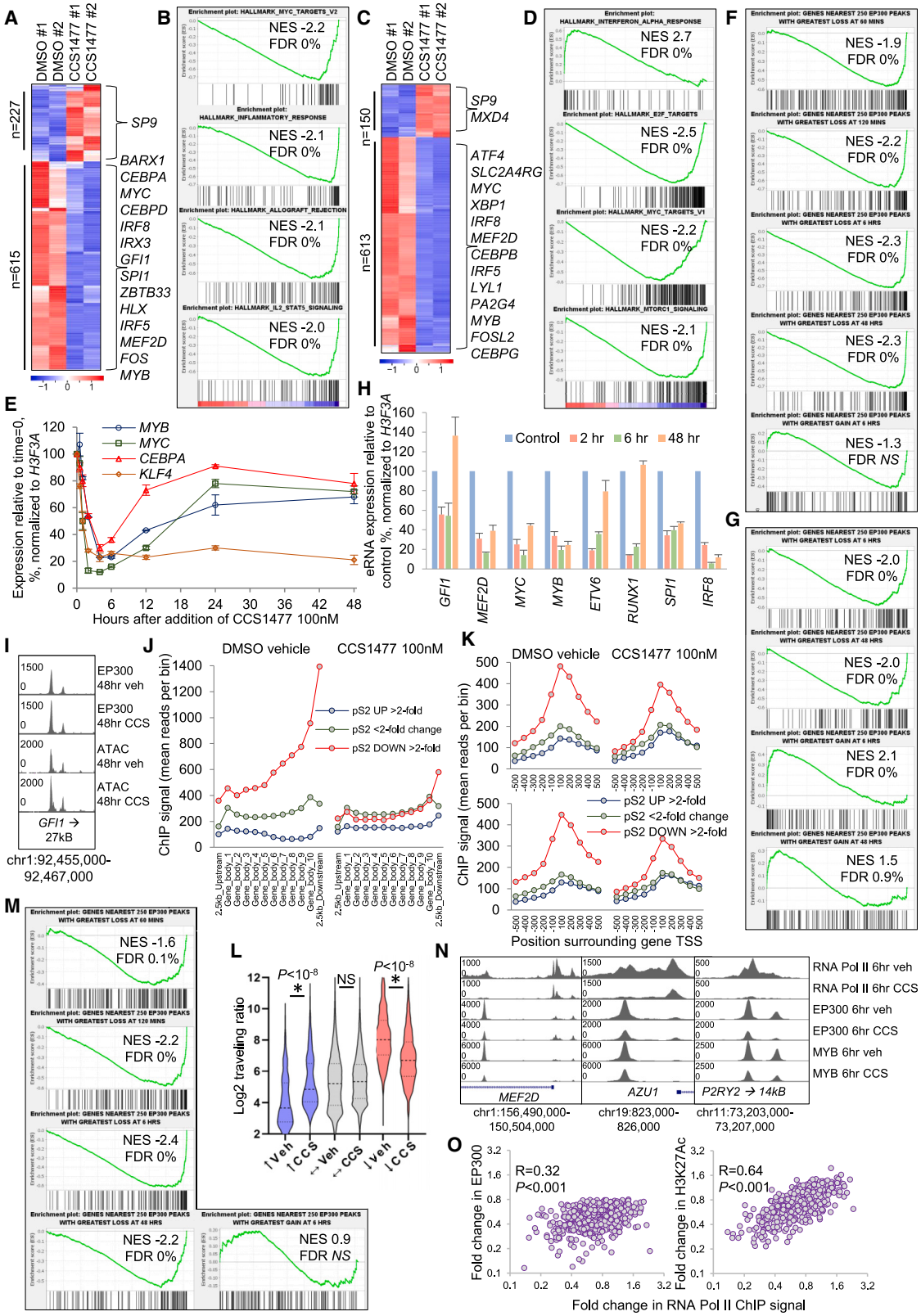

Figure 4. CCS1477-induced changes in EP300 occupancy alter enhancer activity and associated transcriptional program

(A) Heatmap shows differentially expressed genes in THP1 AML cells after 6 h of 100 nM CCS1477; transcription factor genes with high expression (>10 FKPM) are highlighted.

(legend continued on next page)

genes. We made use of gene set enrichment analysis (GSEA) and the Molecular Signatures Database Hallmark Gene Set collection (each of which conveys a specific biological state or process and displays coherent expression)[18] and, in keeping with the GO analysis, noted significant enrichment among downregulated genes of gene sets associated with both MYC, and myeloid lineage identity and function (Figure 4B) (e.g., INFLAMMATORY_RESPONSE, ALLOGRAFT REJECTION).

After 48 h, of 7,361 expressed protein-coding genes, 763 were differentially expressed: 150 were upregulated and 613 downregulated (Figure 4C; Table S3; 1.66-fold change in mean expression). GO analysis revealed significant enrichment of genes with biological process terms "DNA replication" ($p = 10^{-19}$), "DNA repair" ($p = 10^{-15}$), "cholesterol biosynthetic process" ($p = 10^{-7}$), and "inflammatory response" ($p = 10^{-6}$), among downregulated genes. Among upregulated genes, there was enrichment of genes with biological process terms "defense response to virus" ($p = 10^{-7}$) and "cell adhesion" ($p = 10^{-6}$). GSEA showed significant enrichment among downregulated genes of gene sets associated with MYC, cell cycle, and mTORC1 and, among upregulated genes, an INTERFERON_ALPHA_RESPONSE gene set (Figure 4D) which includes genes upregulated in monocyte/macrophage differentiation.

To evaluate this further, we performed qPCR for critical transcription factor genes including *MYB*, *MYC*, and *CEBPA* at multiple time points (Figure 4E). Results were in keeping with the RNA-seq data but further demonstrated, as we had observed for EP300 occupancy (Figure 2), that the rapid and substantial drop in gene expression started within 1 h and deepened over time with a nadir at 4–6 h. The fall in MYB protein levels noted at 6 h (Figure 2E) was due to the fall in *MYB* transcripts: experiments with MG132 to inhibit proteasomal degradation (Figure S5A), or cycloheximide to block translation (Figure S5B), showed no significant difference in MYB degradation or turnover in the presence of CCS1477.

To integrate changes in transcription with sites of EP300 loss, we mapped peak locations to the single nearest gene using Genomic Regions Enrichment of Annotations Tool.[19] Within the limitations of this approach—enhancers do not necessarily control expression of the nearest gene—we noted significant enrichment of genes close to the 250 EP300-binding sites with the greatest loss in ChIP signal at each time point among downregulated genes at 6 h (Figure 4F), whereas there was no enrichment of genes close to the 250 EP300-binding sites with the greatest gain in ChIP signal at 6 h. Likewise, there was significant enrichment of genes close to the 250 EP300-binding sites with the greatest loss or gain in ChIP signal at both 6 and 48 h among genes down- or upregulated respectively at 48 h (Figure 4G). Thus, changes in EP300 occupancy at enhancers mirror changes in expression of nearby genes.

In keeping with this, there was reduced expression of enhancer RNAs (eRNA) at both 2 and 6 h at a selection of sites (Figure 4H), although again this evolved over time. For example, expression of an eRNA close to *GFI1* increased at 48 h (Figure 4H), correlating both with increased expression of *GFI1* (Table S3), increased enhancer occupancy by EP300, and increased chromatin accessibility (Figure 4I).

To further evaluate enhancer activity and the link to transcription of nearby genes, we performed ChIP-seq for RNA polymerase II (total RNA-Pol II), phospho-S5 RNA-Pol II (the initiated form), and phospho-S2 RNA-Pol II (the elongating form) (Figures S5C and S5D) after 6 h. While interpretation is complicated by coincident reduction in MYB protein levels over-and-above the CCS1477-induced displacement of EP300 from chromatin, we nevertheless observed heterogeneous change in ChIP signal for the initiated and elongating forms of RNA-Pol II following exposure of cells to CCS1477. For example, while phospho-S2 and S5 RNA-Pol II ChIP signal was similar in control and drug-treated cells at genes such as *HOXA9*, *HOXA10*, and *CEBPG* (Figure S5C), there was a substantial reduction in phospho-S2 and S5 RNA-Pol II ChIP signal at genes such as *MEF2D*, *CITED4*, and *ZEB2* and the non-coding RNA gene *CCDC26* which sits downstream of *MYC* and within the latter's regulatory control region (Figures S5C–S5E). Available Hi-C data[20] confirmed that MYB-occupied sites where EP300 was evicted made contact with nearby target genes (Figures S5C, S5D, and S6A), providing further evidence for the direct link between CCS1477-induced changes in EP300 enhancer occupancy and activity of nearby genes.

We grouped protein-coding genes into three categories: those where phospho-S2 RNA-Pol II ChIP signal over the distal 50% of the gene increased by > 2-fold ("↑ sites") in CCS1477-treated versus control cells, those where it decreased by > 2-fold ("↓ sites"), and the remainder ("↔ sites") (Figure 4J).

(B) GSEA plots. NES, normalized enrichment score; FDR, false discovery rate.
(C) Heatmap shows differentially expressed genes in THP1 cells after 48 h of 100 nM CCS1477; transcription factor genes are highlighted.
(D) GSEA plots.
(E) Graph shows expression relative to control cells by time for indicated genes in THP1 cells treated with 100 nM CCS1477 (qPCR; mean ± SEM, n = 3).
(F) and (G) GSEA plots.
(H) Graph shows expression relative to control cells by time for enhancer RNAs (eRNAs) transcribed from MYB-bound enhancers in THP1 cells treated with 100 nM CCS1477 (qPCR; mean + SEM, n = 3).
(I) Exemplar ChIP-seq tracks. (J and K) Protein-coding genes were grouped according to whether ChIP signal for phospho-S2 RNA-Pol II over distal 50% of gene body decreased by ≥ 2-fold, increased ≥2-fold, or exhibited little or no change in THP1 cells following 6 h with 100 nM CCS1477. Line plots show (J) mean phospho-S2 RNA-Pol II ChIP signal across gene bodies, (K) mean RNA-Pol II ChIP signal surrounding promoters (upper panel) or mean phospho-S5 RNA-Pol II ChIP signal surrounding promoters (lower panel) for indicated gene groupings in indicated conditions.
(L) Violin plots show distribution, median (thick dotted line) and interquartile range (light dotted lines) of the traveling ratio (log_2) (ratio of distal gene body phospho-S2 RNA-Pol II:RNA-Pol II surrounding promoter) for previously mentioned gene categories in indicated conditions. Significance, unpaired t test. NS, not significant.
(M) GSEA plots.
(N) Exemplar ChIP-seq tracks.
(O) Relationship of fold change in signal surrounding 552 intronic and intergenic "EP300 ↓" sites identified after 6 h of 100 nM CCS1477 and co-occupied at baseline by RNA-Pol II (≥5.6 RPKM), for RNA-Pol II (±300 bps) and EP300 (±300 bps) or H3K27ac (±1000 bps) signal. See also Figures S5 and S6 and Table S3.

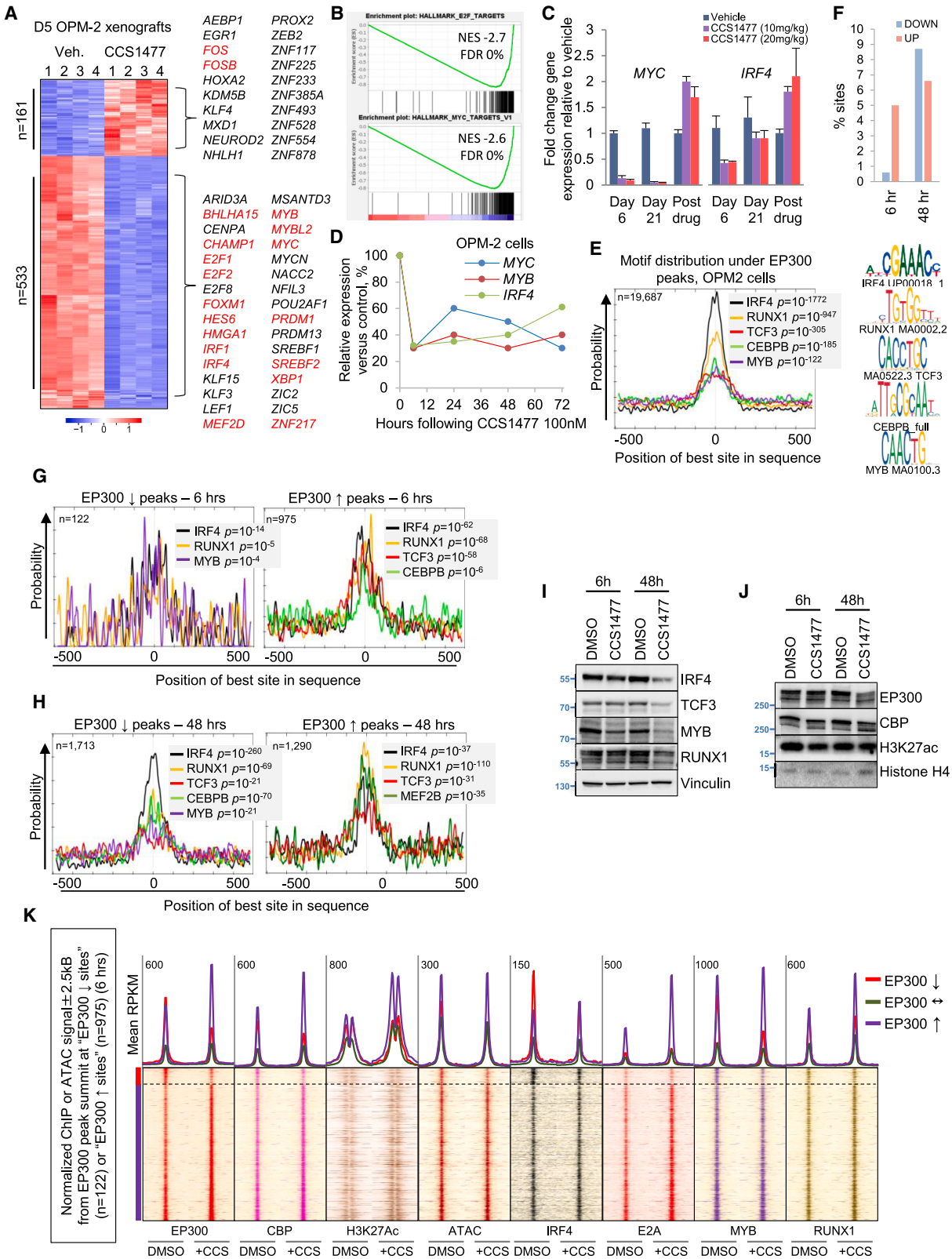

Figure 5. CCS1477 induces loss of EP300 from IRF4 and MYB-bound enhancers in myeloma cells

(A) Heatmap shows differentially expressed genes in OPM-2 myeloma tumors from xenoengrafted mice after five days of 20 mg/kg CCS1477 (see Figure 1J). Transcription factor genes are highlighted; those in red have high expression (among the top 6.5% of all protein coding genes, i.e., ≥6 FPKM).

(legend continued on next page)

Note that while ChIP signal for phospho-S2 RNA-Pol II over distal gene bodies was markedly reduced (by 2.6-fold on average; Figures 4J and S5E), overall there was no significant reduction in ChIP signal for RNA-Pol II at the promoters of the same genes (Figures 4K and S5E) and only a modest albeit significant reduction (by 1.5-fold) surrounding promoters in phospho-S5 RNA-Pol II ChIP signal (Figures 4K and S5E). The ChIP signal traveling ratio (distal gene body phospho-S2 RNA-Pol II:RNA-Pol II surrounding the promoter) was unchanged for the great majority of genes, whereas for those where phospho-S2 RNA-Pol II ChIP signal decreased, the traveling ratio was also decreased, and vice versa (Figure 4L). This indicates that treatment of leukemia cells with CCS1477 induces stalling of RNA-Pol II with failure of transcription elongation at a discrete subset of genes close to enhancers exhibiting EP300 eviction.

To evaluate the link between genes with RNA-Pol II stalling and nearby EP300 and transcription factor-bound regulatory regions, we ranked protein-coding genes according to fold change in phospho-S2 RNA-Pol II ChIP signal across the distal 50% of protein-coding genes after 6 h of treatment with CCS1477 100 nM and performed GSEA. This confirmed an exceptionally strong link between loss of elongating RNA-Pol II and loss of EP300 binding at nearby enhancer sites (Figure 4M). Importantly, among genes with reduced elongating RNA-Pol II after 6 h, there was strong enrichment of genes close to "EP300 ↓" sites identified at 1, 2, 6, and 48 h (Figure 4M). At 552 intronic and intergenic "EP300 ↓" sites identified at 6 h which were co-occupied at baseline by above-threshold levels of RNA-Pol II (≥5.6 RPKM), there was a significant positive correlation of fold change in Pol II occupancy with fold change in occupancy of EP300, CBP, phospho-S2 RNA-Pol II, and phospho-S5 RNA-Pol II, but not MYB (Figures 4N, 4O, and S6B). There was also a significant positive correlation of fold change in Pol II occupancy with fold change in ATAC signal and notably a strong positive correlation with fold change in surrounding H3K27Ac ChIP signal (Figures 4N, 4O, and S6B).

These data directly link CCS147-induced eviction of EP300 from a critical subset of enhancers to reduced enhancer activity and reduced expression of subordinate genes.

CCS1477-induced redistribution of EP300/CBP from IRF4 to TCF3/E2A-occupied sites in myeloma

Next, we considered the response of myeloma cells to CCS1477 and performed comparative bulk RNA-seq analysis of OPM-2 tumors recovered from mice five days after the start of 20 mg/kg CCS1477 treatment (Figure 1J). Considering 8,330 expressed protein-coding genes (i.e., those with mean expression of 0.5 FPKM in the control or drug-treated samples, n = 4 per cohort), 694 were differentially expressed: 161 upregulated and 533 downregulated (Figure 5A; Table S3; $p < 0.005$, t test, 2-fold change in mean expression). GO analysis revealed that among the set of downregulated genes there was significant enrichment of genes mapping to the biological process term "cell division" ($p = 10^{-48}$) and derivative terms. There were no terms among upregulated genes enriched to similar significance. We made use of GSEA and noted significant enrichment among downregulated genes of gene sets associated with both MYC and E2F targets, consistent with drug-induced proliferative arrest (Figure 5B). Among downregulated transcription factor genes were *MYB, MYC*, *IRF4*, *E2F1*, *and FOXM1* (Figure 5A) and we confirmed a subset of these gene expression changes from *in vivo* and *in vitro* material by qPCR (Figures 5C and 5D).

Next, we performed ChIP-seq for EP300 in OPM-2 cells at 6 and 48 h after treatment of cells with 100 nM CCS1477. In steady state, the five strongest centrally enriched transcription factor-binding motif clusters under EP300-binding peaks were those for IRF, Runt, bHLH, bZIP, and MYB/SANT factor classes (Figure 5E). Transcription factor genes *IRF4*, *TCF3* (E2A), *CEBPB*, and *MYB* are exemplar members of these classes with high expression in OPM-2 myeloma cells; *RUNX* genes are expressed at lower level (Table S3).

We again identified sites of substantial differential EP300 occupancy as those with both an absolute change in ChIP signal (±300bps from peak summit) of ≥25 RPKM and a fold change in ChIP signal of ≥1.25. Once more, there was an evolving pattern of altered EP300 occupancy affecting a subset of bound sites (Figure 5F). 6 h following addition of CCS1477 100 nM to OPM-2 cells, there was particular enrichment for IRF4, RUNX1, and MYB motifs at "EP300 ↓" sites and for IRF4, RUNX1, TCF3, and CEBPB at "EP300 ↑" sites (Figure 5G). At 48 h "EP300 ↓" sites, there was much more prominent enrichment for the IRF4 motif, with those for RUNX1, TCF3, IRF4, and MEF2B being enriched under "EP300 ↑" sites (Figure 5H). IRF4 is a critical regulator of plasma cell differentiation.[21,22] Western blotting showed that at 6 h there was minimal change in expression of IRF4, TCF3, RUNX1, EP300, or CBP, although there was once more reduction in MYB protein levels. H3K27Ac levels also remained unchanged. By 48 h, relative to vinculin and histone H4, there was reduced expression of MYB, IRF4, RUNX1, TCF3, and, to lesser extent, EP300 and CBP (Figures 5I and 5J).

To link motif enrichment to EP300, CBP, and transcription factor occupancy as well as histone acetylation and chromatin accessibility, we performed ChIP-seq and ATAC-seq (Figures 5K and 6A–6C). Sites exhibiting reduced EP300 occupancy at 6 h included those within intronic sequences of *FGFR3* which

(B) GSEA plots.
(C) Mean + SEM relative expression of indicated genes in OPM-2 tumors from xenoengrafted mice by time and CCS1477 dose (n = 4 mice/cohort). Post-drug refers to samples collected at euthanasia (days 36 and 39, respectively, for 10 and 20 mg/kg doses).
(D) Mean relative expression (normalized to *GAPDH*) of indicated genes by time in *in vitro* cultured OPM-2 cells after 100 nM CCS1477 (n = 3).
(E) Transcription factor motifs under apices of EP300-binding peaks in OPM-2 cells, with MEME-ChIP *E*-values.
(F) Percentage EP300-binding sites showing changes in EP300 occupancy after 100 nM CCS1477 for 6 and 48 h in OPM-2 cells. MEME-ChIP motif enrichment plots for "EP300 ↓" sites and "EP300 ↑" sites after 6 (G) and 48 h (H) of 100 nM CCS1477.
(I and J) Western blots in OPM-2 cells treated for 6 and 48 h with 100 nM CCS1477.
(K) Heatmaps show ATAC or ChIP signal ±2.5kB from the summit of EP300-binding peaks in OPM-2 cells treated for 6 h with 100 nM CCS1477 for indicated factors in indicated conditions. EP300-binding sites are grouped in ranked order of loss ("EP300 ↓" sites) or gain ("EP300 ↑" sites) of EP300 ChIP signal from those sites after 6 h of 100 nM CCS1477. Graphs above heatmaps show mean ChIP signal for indicated peak group. See also Figure S6.

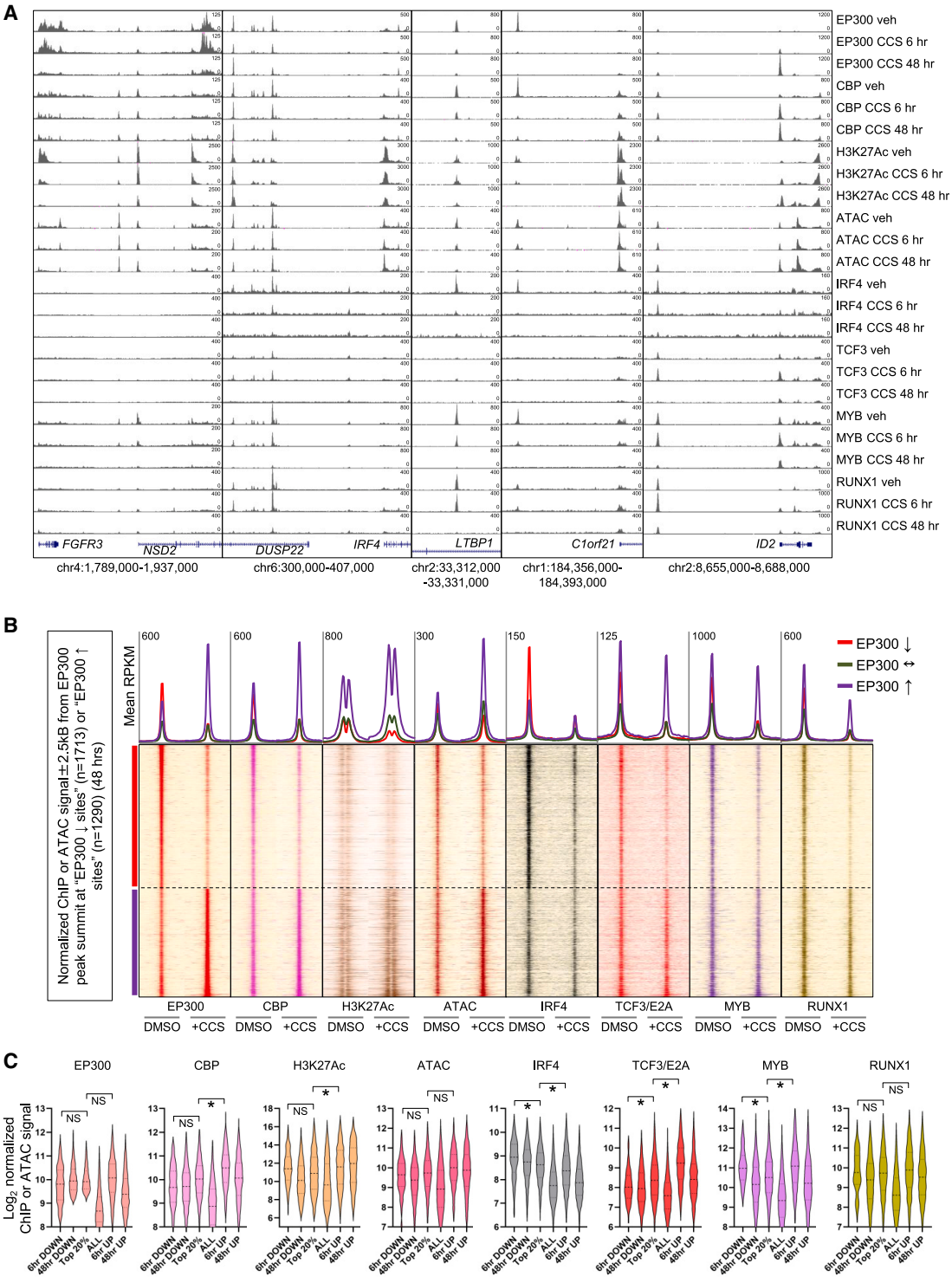

Figure 6. Longer CCS1477 treatment induces redistribution of EP300 in OPM-2 myeloma cells

(A) Exemplar ChIP-seq and ATAC-seq tracks.

(B) Heatmaps show ATAC or ChIP signal ±2.5 kB from the summit of EP300-binding peaks in OPM-2 myeloma cells after 48 h of 100 nM CCS1477 for indicated factors in indicated conditions. EP300-binding sites are grouped in ranked order of loss ("EP300 ↓" sites) or gain ("EP300 ↑" sites) of EP300 ChIP signal from those sites after 48 h of 100 nM CCS1477. Graphs above heatmaps show mean ChIP signal for the indicated peak group.

(C) Violin plots show distribution, median (thick dotted line) and interquartile range (light dotted lines) of ChIP signal for indicated proteins or ATAC signal at indicated genomic regions in OPM-2 cells. Statistical significance, one-way ANOVA, Tukey post hoc test (* indicates both $p < 0.01$ and >1.2 mean fold change in ChIP signal; NS, not significant). See also Figure S6.

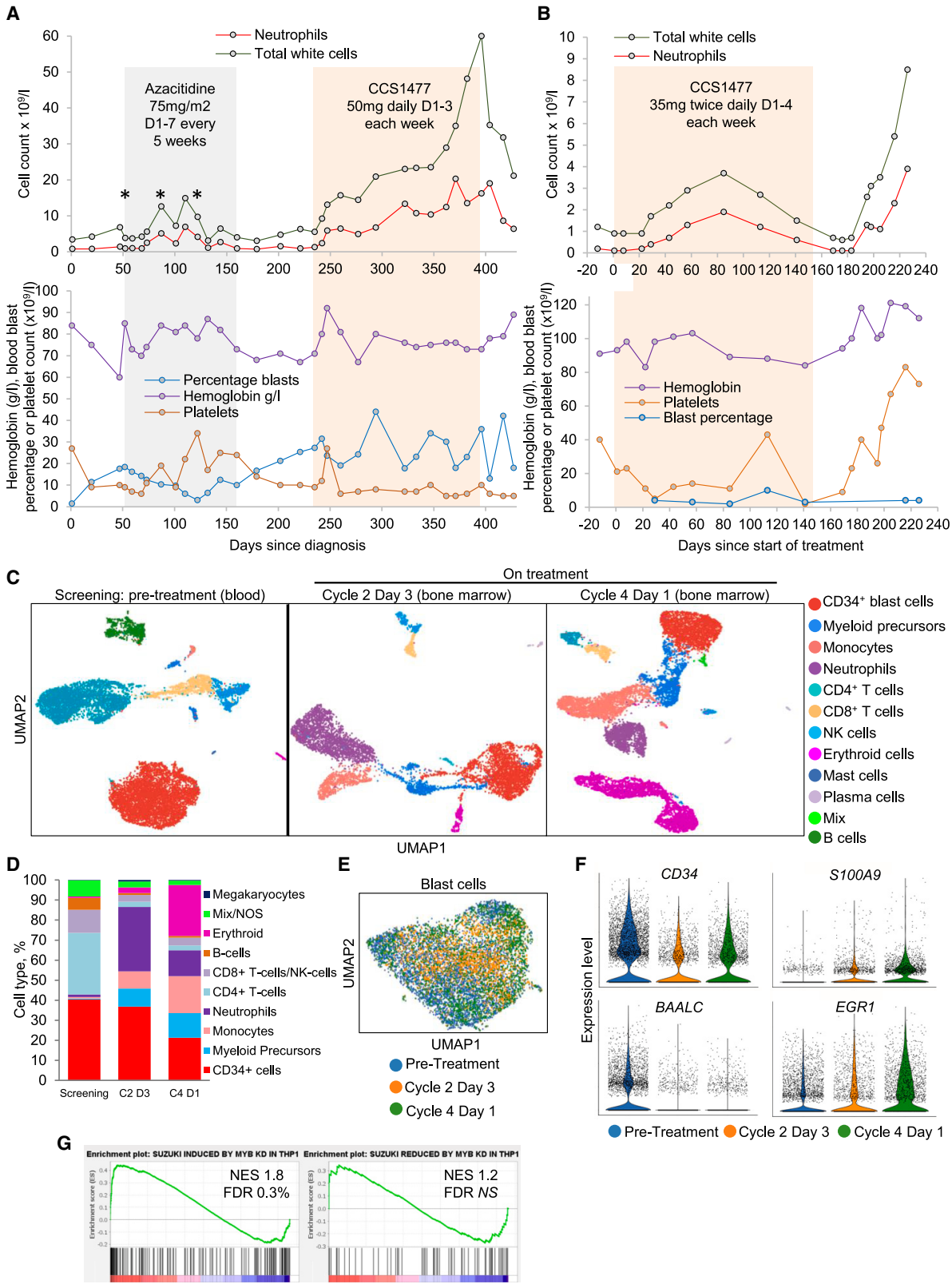

Figure 7. CCS1477-induced granulocytic differentiation responses in poor prognosis patients with AML

(A) and (B) Exemplar disease and treatment response trajectories; in (A) asterisks indicate timing of azacitidine cycles.

(C) UMAP visualizations by time for samples from the patient in Figure S7A.

(legend continued on next page)

is under the control of the active IGH promoter in the intergenic t(4; 14) exhibited by OPM-2 cells; and IRF4- and MYB-occupied intronic sequences within *DUSP22* which are known to make contact with the IRF4 promoter in Hi-C analyses of spleen cells[20] (Figure 6A). Compared to the strongest 20% of EP300-binding sites in steady state, and in keeping with the motif analysis (Figure 5G), "EP300 ↓" sites at 6 h exhibited significantly stronger ChIP signal for both IRF4 and MYB. In contrast, "EP300 ↑" sites at 6 h exhibited in steady state significantly lower ChIP signal for IRF4 and significantly higher ChIP signal for TCF3/E2A, MYB, CBP and H3K27Ac, as well as for ATAC-seq signal (Figures 5K and 6C). At "EP300 ↓" sites, there was loss of IRF4 and MYB ChIP signal, with reduced chromatin accessibility (Figure 5K) whereas at "EP300 ↑" sites there was increased histone acetylation, TCF3/E2A, and RUNX1 occupancy (Figure 5K). While MYB occupies acetylated, open sites in OPM-2 cells as it does in THP1 cells (Figure 3A), it likely plays a less significant role perhaps related to different levels of expression, or co-expression of alternate transcriptional regulators.

By 48 h, there was a more extensive redistribution of EP300 binding (Figures 5F and 6A–6C) with respective reductions or increases in ATAC-seq signal and ChIP signal for EP300, CBP, and H3K27Ac at "EP300 ↓" and "EP300 ↑" sites (Figure 6B). In keeping with western blotting (Figures 5I and 5J), ChIP signal for all four transcription factors was reduced, although the relative fall was least at "EP300 ↑" sites. Fold change in ChIP signal for EP300 again correlated strongly genome-wide with fold change in CBP (Figure S6C) and H3K27Ac (Figure S6D) ChIP signals, as well as fold change in ATAC-seq signal (Figure S6E). Likewise, strength of ChIP-seq signal for CBP and EP300 at baseline also correlated strongly genome-wide (Figure S6F) indicating that as for THP1 cells, EP300 and CBP occupy the same sites on chromatin in OPM-2 cells with similar strength and are lost from the same subset of genomic regions after addition of CCS1477. As for *MYB* KD in THP1 cells, we observed that *IRF4* KD in OPM-2 cells also induced cell-cycle arrest (Figures S6G and S6H).

Altogether, these data demonstrate that in OPM-2 myeloma cells CCS1477 induces within hours a redistribution of EP300/CBP away from both *FGFR3* at the t(4; 14) breakpoint and sites occupied by IRF4, and toward sites occupied by TCF3/E2A.

Evidence of activity of CCS1477 in MDS/AML

CCS1477 is in phase 1 evaluation (NCT04068597) in relapsed or refractory hematologic malignancies, a challenging group of patients who have exhausted standard-of-care therapies. The following selected clinical cases demonstrate that CCS1477 monotherapy shows clinical activity, in keeping with our preclinical data.

A patient in his 70s with myelodysplasia with excess blasts 2 (MDS-EB2), a 45XY, del5q, −7 karyotype, and an ASXL1 p.Tyr591* variant received three cycles of azacitidine but progressed to AML. The six months following diagnosis were complicated by four admissions for neutropenic sepsis. While initiation of therapy with oral CCS1477 led to a brief admission for management of splenic infarction in the first week of treatment, he remained well for the next five months with no infective episodes. Most notably, CCS1477 treatment was associated with a substantial increase in blood neutrophil count (Figure 7A), which may have been responsible for the reduced frequency of septic episodes. Treatment was later discontinued in view of a rising total leukocyte count; hydroxycarbamide was commenced but the patient died shortly thereafter of AML.

A patient in his 60s with normal karyotype AML was treated with three cycles of daunorubicin and cytarabine before relapsing six months later. He then received fludarabine, idarubicin, and high-dose cytarabine salvage therapy. At second relapse, ten months later he received CCS1477. There were two episodes of neutropenic sepsis at the start and the end of treatment when the neutrophil count was $<0.5\times10^9$/l; the latter resulted in study withdrawal. Treatment was well tolerated and again characterized by a significant increase in blood neutrophil count, sustained for 3–4 months. Intriguingly, in the three months following therapy withdrawal, in the absence of further therapy, there was a further unexpected recovery of neutrophil and platelet count (Figure 7B).

Trial samples were available from a third patient (a man in his 70s with MDS-EB2 and a 46XY del12p karyotype who had failed azacitidine in view of prolonged, severe cytopenias) who also exhibited a neutrophil response to CCS1477 treatment (Figure S7A). This permitted single-cell RNA-seq analysis of blood mononuclear cells from screening (marrow was unavailable) and bone marrow following two and four months of treatment. As expected, based on the profoundly cytopenic blood counts (Figure S7A) in the screening sample, cluster annotation showed there to be plentiful myeloblasts but few maturing and mature myeloid cells (Figure 7C). By contrast, in the bone marrow samples during treatment (where there was recovery to normal levels of peripheral blood neutrophils), there was substantial myeloid activity (Figures 7C and 7D). Dimensionality reduction and visualization using uniform manifold approximation and projection and unsupervised clustering showed that while blast cell transcriptomes clustered together at all time points (Figures 7E, S7B, and S7C), there were clear differences in gene expression within the blast cluster. Consistent with our *in vitro* results demonstrating that CCS1477 promotes differentiation of primary AML samples across a range of molecular subtypes, there was downregulation of exemplar stem cell genes such as *CD34* and *BAALC*, and upregulation of differentiation genes *S100A9* and *EGR1* (Figure 7F). Indeed, when single-cell transcriptomes within the blast cluster were integrated and ranked by fold change in expression, GSEA revealed upregulation of a multilineage differentiation program and downregulation of a stem cell program during treatment with CCS1477 (Figure S7D). Furthermore, and in keeping with our *in vitro* cell line analyses, there was also upregulation of genes induced by *MYB* KD in THP1 AML cells (Figure 7G).

(D) Proportional cell type composition.
(E) UMAP visualization of blast cells by time.
(F) Violin plots show expression of indicated genes by time.
(G) GSEA plots. See also Figure S7.

Thus, in selected neutropenic patients with AML with relapsed or refractory high-risk disease, CCS1477 monotherapy in addition to being well tolerated, induced differentiation responses in blast populations and in blood counts that were potentially therapeutically useful.

Evidence of activity of CCS1477 in multiple myeloma

Patients with myeloma who have failed treatment with all three major drug classes (proteasome inhibitors, immunomodulatory drugs, and anti-CD38 antibodies) have exceptionally poor prognosis.[23] As for AML, selected case studies illustrate that CCS1477 monotherapy shows clinical activity in keeping with our preclinical data. A patient in his 60s was treated over 18 years with six lines of therapy for light-chain myeloma, receiving dexamethasone, vincristine, doxorubicin, two melphalan autografts, bortezomib, lenalidomide, radiotherapy to a sacral plasmacytoma, pomalidomide, and bendamustine with thalidomide. At enrollment, there was widespread but patchy myeloma throughout the skeleton. FISH analysis showed an IGH gene rearrangement with an unknown partner gene and gain of chromosome 1q21. Despite rapidly progressive disease during screening, CCS1477 monotherapy conferred a sustained reduction in urinary free light chains over five months before disease progression and study withdrawal (Figure 8A). Treatment was free of significant complication save for an admission shortly after starting therapy for fever and low back pain, and moderate thrombocytopenia at the beginning of cycle 3 where treatment was held for a week.

A patient in his 50s treated over nine years for kappa light-chain myeloma (with an IGH gene rearrangement with an unknown partner gene) with four lines of therapy including bortezomib, cyclophosphamide, thalidomide, two melphalan autografts, ixazomib, lenalidomide, isatuximab, and pomalidomide, exhibited progressive disease as evidenced by rising serum kappa light chains. Oral therapy at the recommended phase 2 dose of 35 mg twice daily for four days each week, which was well tolerated, induced substantial falls in both serum and urinary free kappa light chains sustained past 12 months (Figure 8B).

A third patient in her 60s with IgG kappa myeloma (with no evidence of an IGH rearrangement by FISH) had received bortezomib, daratumumab, and a melphalan autograft over six years and was unable to tolerate thalidomide, lenalidomide, or panobinostat. She exhibited a sustained response to CCS1477 over 11 months which began to wane with time (Figure S8A). A fourth patient in her 60s with light-chain myeloma (with no evidence of an IGH rearrangement by FISH) had received over 12 years thalidomide, cyclophosphamide, bortezomib, two melphalan autografts, ixazomib, lenalidomide, pomalidomide, and isatuximab. CCS1477 monotherapy was sufficient to maintain stable disease past 12 months. In each of these four cases, CCS1477 induced a modest thrombocytopenia without adversely affecting hemoglobin or white cells (Figures 8A, 8B, S8A, and S8B).

Thus, in line with our preclinical data, CCS1477 induces therapeutic responses in selected patients with heavily pre-treated myeloma.

In vivo synergy of CCS1477 with standard-of-care agents in MDS/AML and multiple myeloma

Finally, while the previously described case histories represent encouraging evidence of single-agent activity in some cases, most successful regimens in blood cancer therapy are combinatorial. We therefore evaluated the activity of CCS1477 in xenograft models in combination with existing standard-of-care agents. Azacitidine and CCS1477 in particular demonstrated synergistic growth inhibitory activity in the MOLM16 model (Figure 8C), as did venetoclax in MOLM16 and MV(4; 11) models (Figures 8D and 8E). In an OPM-2 xenograft model, there was additive or synergistic growth inhibitory activity with each of bortezomib, lenalidomide, and vorinostat in combination with CCS1477 (Figure 8F). Combination treatment was not associated with significant reduction in mean body weight of any cohort, save for mice treated with the azacitidine/CCS1477 combination where there was a 5%–10% reduction in mean body weight over the 14-day treatment (Figures S8C–S8F).

DISCUSSION

While selective EP300/CBP bromodomain inhibitors are reported, only CCS1477 and FT7051[24] have moved to clinical evaluation. The *in vitro* cellular phenotypes—growth arrest and differentiation with minimal apoptosis—differ from those observed in leukemia cells treated with BET bromodomain inhibitors where apoptosis predominates.[25] Along with our BROMOscan data, this emphasizes that CCS1477 exhibits distinctive activity.

In AML and myeloma cells, CCS1477 induced EP300/CBP redistribution away from sites occupied by cell-type-specific master transcription factors, leading to downregulation of the oncogenic program. In AML, MYB is a critical component of the *MLL*-translocated leukemia stem cell program;[26,27] we observed remarkable responses to CCS1477 in experimentally initiated murine *MLL* leukemias. In THP1 AML cells (which exhibit a t(9; 11) *MLL* translocation), EP300/CBP is strongly and proportionally recruited to MYB-occupied sites and, within 1 h of CCS1477 exposure, with MYB protein levels unchanged, EP300 eviction from a subset of strongly acetylated, open enhancers was already detected. We hypothesize that through bromodomain binding, CCS1477 reduces the efficiency of EP300/CBP recruitment to some of its most strongly bound sites thereby reducing enhancer activity and expression of subordinate genes. In THP1 cells, this leads to a cascading decrease in activity of the MYB-centered enhancer network and abrupt reduction in transcription of subordinate genes. MYB protein, with its short half-life, is transiently depleted as a consequence of reduced transcripts. While MYB interacts with EP300/CBP through the EP300/CBP KIX domain, the EP300/CBP bromodomain is required for MYB acetylation which increases DNA binding and transactivation.[28,29] Thus, CCS1477 may potentially disrupt interaction of the EP300/CBP bromodomain with acetylated MYB, although recruitment of EP300/CBP to chromatin by other acetylated proteins may also be important.

Intriguingly, genes with reduced expression include *MEF2D* and *IRF8* which form a core regulatory circuit in AML;[10,30] our data suggest this circuits sits downstream of MYB, which may in AML be present on chromatin as part of an aberrant complex.[31] Our data also suggest that MYB-bound enhancers promote RNA-Pol II pause release from subordinate promoters, perhaps in collaboration with MYC.[32] Furthermore, loss of EP300 and MYB from MYB-bound enhancers is associated

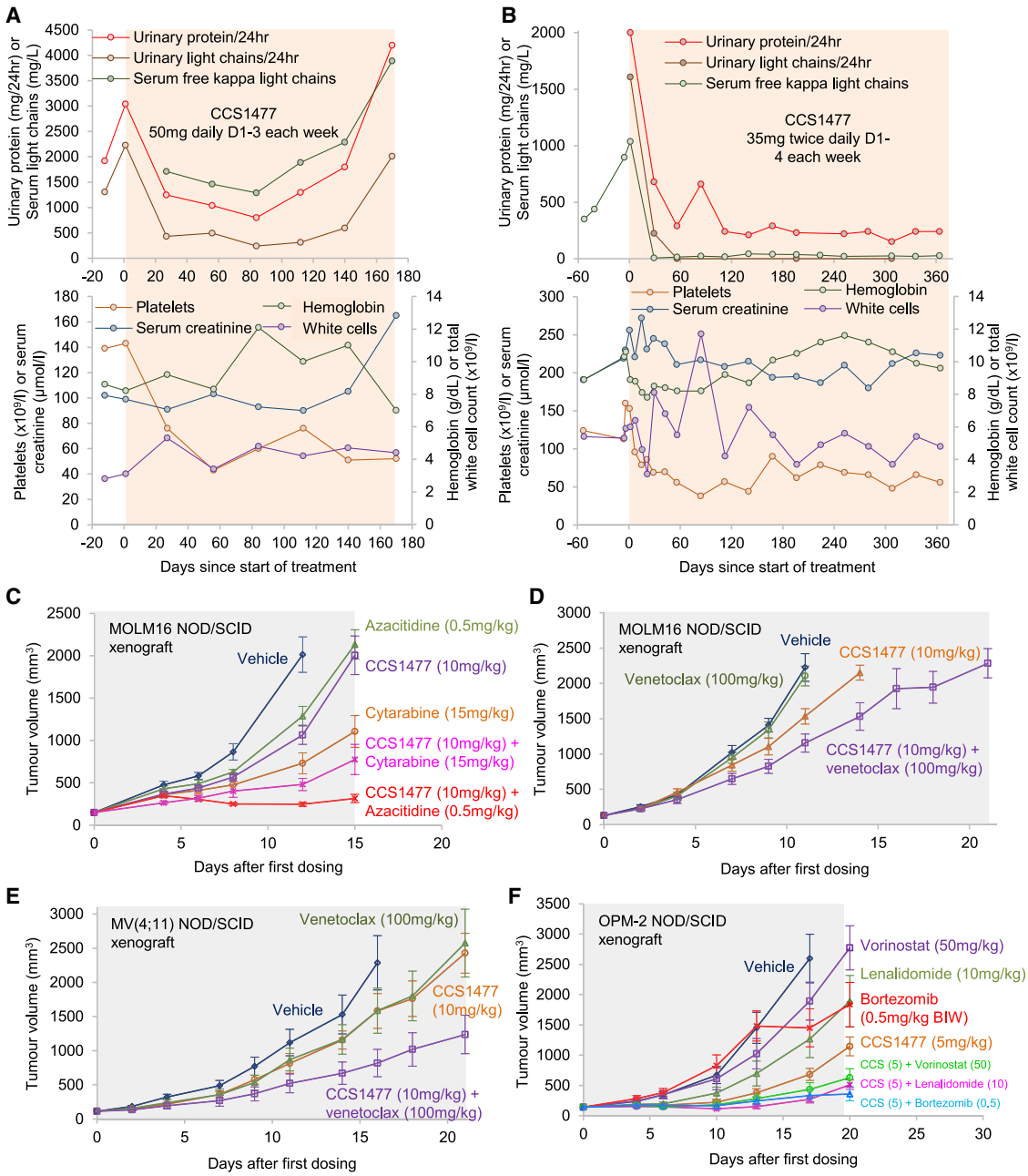

Figure 8. Responses in patients with heavily pre-treated myeloma and evaluation of combination therapy with standard-of-care agents

(A) and (B) Exemplar disease and treatment response trajectories. Growth curves show mean + SEM tumor volume in xenograft experiments (n = 5 mice/cohort) with (C), (D) MOLM16 AML cells, (E) MV(4; 11) AML cells, and (F) OPM-2 myeloma cells with CCS1477, the indicated standard-of-care agents, or a combination of the two. See also Figure S8.

with reduced chromatin accessibility although this seems peculiar to EP300/CBP bromodomain rather than catalytic inhibitors.[33]

In OPM-2 myeloma cells, CCS1477 rapidly reduced dense EP300 occupancy at intronic *FGFR3* sites close to the t(4; 14) breakpoint, and at sites occupied by the myeloma oncogenic factor IRF4. There follows a redistribution toward sites occupied by TCF3/E2A, an essential B cell lineage transcription factor.[34] IRF4 and MYC function in an autoregulatory circuit in myeloma[8,22] and our data indicate that CCS1477 downregulates this activity, as has been reported for CBP30 in LP-1 myeloma cells.[8]

Our findings contrast with those for EP300/CBP bromodomain tool compound GNE-049 in MOLM16 AML cells and LP1 myeloma cells. While sensitivity across hematologic cell line models was noted, global reduction in production of enhancer RNAs and H3K27Ac (but not H3K18Ac) was reported, the latter within 5 min, but without changes in EP300 occupancy.[35] The

reasons for these marked differences between studies remain unclear.

A feature of our preclinical studies was dose dependency: at higher doses in xenograft models tumors regressed, with resumed growth taking 10 days after drug discontinuation. Our data highlight extensive enhancer rewiring and the resultant epigenetic barrier to tumor growth as a potential explanation.

While preclinical studies permit sustained exposure of target cells *in vitro* and *in vivo* to fixed drug concentrations, in early-phase trials safety is paramount. Thrombocytopenia was dose limiting in animal models and so an intermittent dosing strategy was adopted in humans. Typical C_{max} plasma concentrations achieved for 35 and 50 mg oral doses are 1400–2400 nM with T_{max} of 1 h and t(1/2) of 6 h which are comparable to doses achieved preclinically.

Finally, selected clinical cases demonstrate that EP300/CBP bromodomain targeting has therapeutic potential. Patients with relapsed or refractory AML often die as a result of infection associated with severe neutropenia. In some patients, prominent granulocytic responses were noted, with CCS1477 inducing up-regulation of a differentiation program within the blast population. In a subset of heavily pre-treated patients with multiple myeloma, there was stabilization or even substantial reduction in serum and/or urinary free light chains, in some cases sustained past 12 months. These encouraging signs in a challenging population together with evidence of synergistic activity in preclinical AML and myeloma models of CCS1477 with standard-of-care agents set the scene for future clinical development. In AML, CCS1477 will be tested in combination with azacitidine and venetoclax, and in myeloma in combination with pomalidomide and dexamethasone. Future predictive biomarker studies will help define populations most likely to benefit from CCS1477.

STAR★METHODS

Detailed methods are provided in the online version of this paper and include the following:

- KEY RESOURCES TABLE
- RESOURCE AVAILABILITY
  - Lead contact
  - Materials availability
  - Data and code availability
- EXPERIMENTAL MODEL AND STUDY PARTICIPANT DETAILS
  - Animal studies
  - Human participants
  - Cell lines
  - Primary cells
- METHOD DETAILS
  - Flow cytometry, apoptosis and cell cycle analysis
  - Virus particle manufacture
  - shRNA cloning
  - Western blotting
  - RNA sequencing
  - Single cell RNA sequencing (scRNA) library preparation and sequencing
  - 10x Genomics scRNA sequencing processing and analysis
  - Quantitative PCR analysis
  - Chromatin immunoprecipitation (ChIP) and next generation sequencing
  - ChIP-qPCR
  - ATAC sequencing
  - Bromodomain assays
- QUANTIFICATION AND STATISTICAL ANALYSIS
  - Gene set enrichment analysis
  - Statistics

SUPPLEMENTAL INFORMATION

Supplemental information can be found online at https://doi.org/10.1016/j.ccell.2023.11.001.

ACKNOWLEDGMENTS

This study was supported by Cancer Research UK (C5759/A20971 and C5759/A27412; L.N., F.M.R.A., B.R., J.A.C., A.M.-D., F. Camera, F. Ciceri, and T.C.P.S.), CellCentric (G.J.S.), Imago Biosciences (N.J.B.), Leukaemia UK (2020/JGF/005, B.W.), Blood Cancer UK (15030, D.H.W.), and Oglesby Charitable Trust (D.H.W.). We thank Jeff Barry, Wolfgang Breitwieser, Gillian Newton, Amy Priestman, John Weightman, Biological Resources Unit, and Priyanka Bhattacharya for technical support. Clinical data generation was supported by NIHR Manchester Clinical Research Facility and Manchester Experimental Cancer Medicine Center.

AUTHOR CONTRIBUTIONS

Experiments, L.N., G.J.S., N.J.B., J.A.C., B.R., B.W., A.M.-D., O.S., F. Camera, F. Ciceri, and T.C.P.S.; data analysis, N.B., L.N., G.J.S., N.J.B., F.M.R.A., and T.C.P.S.; compound development and production, N.P. and W.W.; clinical data and analysis, T.K., K.C., W.W., N.B., D.H.W., J.C., E.S., M.C., and T.C.P.S.; manuscript writing, L.N., G.J.S., K.F., N.B., and T.C.P.S. All authors approved the final version.

DECLARATION OF INTERESTS

W.W. and N.P.: employees, board directors, and shareholders of CellCentric Ltd; N.P.: inventor on CCS1477 patents; N.B., T.K., K.F., and K.C.: employees and shareholders of CellCentric Ltd.

Received: July 8, 2022
Revised: August 7, 2023
Accepted: November 1, 2023
Published: November 22, 2023

REFERENCES

1. Dyson, H.J., and Wright, P.E. (2016). Role of Intrinsic Protein Disorder in the Function and Interactions of the Transcriptional Coactivators CREB-binding Protein (CBP) and p300. J. Biol. Chem. *291*, 6714–6722.
2. Attar, N., and Kurdistani, S.K. (2017). Exploitation of EP300 and CREBBP Lysine Acetyltransferases by Cancer. Cold Spring Harb. Perspect. Med. *7*, a026534.
3. Weinert, B.T., Narita, T., Satpathy, S., Srinivasan, B., Hansen, B.K., Schölz, C., Hamilton, W.B., Zucconi, B.E., Wang, W.W., Liu, W.R., et al. (2018). Time-Resolved Analysis Reveals Rapid Dynamics and Broad Scope of the CBP/p300 Acetylome. Cell *174*, 231–244.e12.
4. Delvecchio, M., Gaucher, J., Aguilar-Gurrieri, C., Ortega, E., and Panne, D. (2013). Structure of the p300 catalytic core and implications for chromatin targeting and HAT regulation. Nat. Struct. Mol. Biol. *20*, 1040–1046.
5. Meyer, S.N., Scuoppo, C., Vlasevska, S., Bal, E., Holmes, A.B., Holloman, M., Garcia-Ibanez, L., Nataraj, S., Duval, R., Vantrimpont, T., et al. (2019). Unique and Shared Epigenetic Programs of the CREBBP and EP300

Acetyltransferases in Germinal Center B Cells Reveal Targetable Dependencies in Lymphoma. Immunity *51*, 535–547.e9.

6. Breen, M.E., and Mapp, A.K. (2018). Modulating the masters: chemical tools to dissect CBP and p300 function. Curr. Opin. Chem. Biol. *45*, 195–203.
7. Welti, J., Sharp, A., Brooks, N., Yuan, W., McNair, C., Chand, S.N., Pal, A., Figueiredo, I., Riisnaes, R., Gurel, B., et al. (2021). Targeting the p300/CBP Axis in Lethal Prostate Cancer. Cancer Discov. *11*, 1118–1137.
8. Conery, A.R., Centore, R.C., Neiss, A., Keller, P.J., Joshi, S., Spillane, K.L., Sandy, P., Hatton, C., Pardo, E., Zawadzke, L., et al. (2016). Bromodomain inhibition of the transcriptional coactivators CBP/EP300 as a therapeutic strategy to target the IRF4 network in multiple myeloma. Elife *5*, e10483.
9. Picaud, S., Fedorov, O., Thanasopoulou, A., Leonards, K., Jones, K., Meier, J., Olzscha, H., Monteiro, O., Martin, S., Philpott, M., et al. (2015). Generation of a Selective Small Molecule Inhibitor of the CBP/p300 Bromodomain for Leukemia Therapy. Cancer Res. *75*, 5106–5119.
10. Cao, Z., Budinich, K.A., Huang, H., Ren, D., Lu, B., Zhang, Z., Chen, Q., Zhou, Y., Huang, Y.H., Alikarami, F., et al. (2021). ZMYND8-regulated IRF8 transcription axis is an acute myeloid leukemia dependency. Mol. Cell *81*, 3604–3622.e10.
11. Machanick, P., and Bailey, T.L. (2011). MEME-ChIP: motif analysis of large DNA datasets. Bioinformatics *27*, 1696–1697.
12. Pattabiraman, D.R., and Gonda, T.J. (2013). Role and potential for therapeutic targeting of MYB in leukemia. Leukemia *27*, 269–277.
13. Maiques-Diaz, A., Spencer, G.J., Lynch, J.T., Ciceri, F., Williams, E.L., Amaral, F.M.R., Wiseman, D.H., Harris, W.J., Li, Y., Sahoo, S., et al. (2018). Enhancer Activation by Pharmacologic Displacement of LSD1 from GFI1 Induces Differentiation in Acute Myeloid Leukemia. Cell Rep. *22*, 3641–3659.
14. Simeoni, F., Romero-Camarero, I., Camera, F., Amaral, F.M.R., Sinclair, O.J., Papachristou, E.K., Spencer, G.J., Lie-A-Ling, M., Lacaud, G., Wiseman, D.H., et al. (2021). Enhancer recruitment of transcription repressors RUNX1 and TLE3 by mis-expressed FOXC1 blocks differentiation in acute myeloid leukemia. Cell Rep. *36*, 109725.
15. ENCODE Project Consortium, Moore, J.E., Purcaro, M.J., Pratt, H.E., Epstein, C.B., Shoresh, N., Adrian, J., Kawli, T., Davis, C.A., Dobin, A., et al. (2020). Expanded encyclopaedias of DNA elements in the human and mouse genomes. Nature *583*, 699–710.
16. Rousseau, P., Masternak, K., Krawczyk, M., Reith, W., Dausset, J., Carosella, E.D., and Moreau, P. (2004). In vivo, RFX5 binds differently to the human leucocyte antigen-E, -F, and -G gene promoters and participates in HLA class I protein expression in a cell type-dependent manner. Immunology *111*, 53–65.
17. Sherman, B.T., Hao, M., Qiu, J., Jiao, X., Baseler, M.W., Lane, H.C., Imamichi, T., and Chang, W. (2022). DAVID: a web server for functional enrichment analysis and functional annotation of gene lists (2021 update). Nucleic Acids Res. *50*, W216–W221.
18. Liberzon, A., Subramanian, A., Pinchback, R., Thorvaldsdóttir, H., Tamayo, P., and Mesirov, J.P. (2011). Molecular signatures database (MSigDB) 3.0. Bioinformatics *27*, 1739–1740.
19. McLean, C.Y., Bristor, D., Hiller, M., Clarke, S.L., Schaar, B.T., Lowe, C.B., Wenger, A.M., and Bejerano, G. (2010). GREAT improves functional interpretation of cis-regulatory regions. Nat. Biotechnol. *28*, 495–501.
20. Wang, Y., Song, F., Zhang, B., Zhang, L., Xu, J., Kuang, D., Li, D., Choudhary, M.N.K., Li, Y., Hu, M., et al. (2018). The 3D Genome Browser: a web-based browser for visualizing 3D genome organization and long-range chromatin interactions. Genome Biol. *19*, 151.
21. Kortüm, K.M., Zhu, Y.X., Shi, C.X., Jedlowski, P., and Stewart, A.K. (2015). Cereblon binding molecules in multiple myeloma. Blood Rev. *29*, 329–334.
22. Shaffer, A.L., Emre, N.C.T., Lamy, L., Ngo, V.N., Wright, G., Xiao, W., Powell, J., Dave, S., Yu, X., Zhao, H., et al. (2008). IRF4 addiction in multiple myeloma. Nature *454*, 226–231.
23. Bal, S., Malek, E., Kansagra, A., Usmani, S.Z., Vij, R., Godby, K.N., Cornell, R.F., Kang, Y., Umyarova, E., Giri, S., et al. (2022). Treatment outcomes of triple class refractory multiple myeloma: a benchmark for new therapies. Leukemia *36*, 877–880.
24. Armstrong, A.J., Gordon, M.S., Reimers, M.A., Hussain, A., Patel, V.G., Lam, E.T., Sedkov, A., Potter, V., and Shore, N. (2021). Abstract P202: Initial findings from an ongoing first-in-human phase 1 study of the CBP/p300 inhibitor FT-7051 in men with metastatic castration-resistant prostate cancer. Mol. Cancer Therapeut. *20*, P202.
25. Zuber, J., Shi, J., Wang, E., Rappaport, A.R., Herrmann, H., Sison, E.A., Magoon, D., Qi, J., Blatt, K., Wunderlich, M., et al. (2011). RNAi screen identifies Brd4 as a therapeutic target in acute myeloid leukaemia. Nature *478*, 524–528.
26. Hess, J.L., Bittner, C.B., Zeisig, D.T., Bach, C., Fuchs, U., Borkhardt, A., Frampton, J., and Slany, R.K. (2006). c-Myb is an essential downstream target for homeobox-mediated transformation of hematopoietic cells. Blood *108*, 297–304.
27. Somervaille, T.C.P., Matheny, C.J., Spencer, G.J., Iwasaki, M., Rinn, J.L., Witten, D.M., Chang, H.Y., Shurtleff, S.A., Downing, J.R., and Cleary, M.L. (2009). Hierarchical maintenance of MLL myeloid leukemia stem cells employs a transcriptional program shared with embryonic rather than adult stem cells. Cell Stem Cell *4*, 129–140.
28. Tomita, A., Towatari, M., Tsuzuki, S., Hayakawa, F., Kosugi, H., Tamai, K., Miyazaki, T., Kinoshita, T., and Saito, H. (2000). c-Myb acetylation at the carboxyl-terminal conserved domain by transcriptional co-activator p300. Oncogene *19*, 444–451.
29. Sano, Y., and Ishii, S. (2001). Increased affinity of c-Myb for CREB-binding protein (CBP) after CBP-induced acetylation. J. Biol. Chem. *276*, 3674–3682.
30. Harada, T., Heshmati, Y., Kalfon, J., Perez, M.W., Xavier Ferrucio, J., Ewers, J., Hubbell Engler, B., Kossenkov, A., Ellegast, J.M., Yi, J.S., et al. (2022). A distinct core regulatory module enforces oncogene expression in KMT2A-rearranged leukemia. Genes Dev. *36*, 368–389.
31. Takao, S., Forbes, L., Uni, M., Cheng, S., Pineda, J.M.B., Tarumoto, Y., Cifani, P., Minuesa, G., Chen, C., Kharas, M.G., et al. (2021). Convergent organization of aberrant MYB complex controls oncogenic gene expression in acute myeloid leukemia. Elife *10*, e65905.
32. Rahl, P.B., Lin, C.Y., Seila, A.C., Flynn, R.A., McCuine, S., Burge, C.B., Sharp, P.A., and Young, R.A. (2010). c-Myc regulates transcriptional pause release. Cell *141*, 432–445.
33. Ebrahimi, A., Sevinç, K., Gürhan Sevinç, G., Cribbs, A.P., Philpott, M., Uyulur, F., Morova, T., Dunford, J.E., Göklemez, S., Arı, Ş., et al. (2019). Bromodomain inhibition of the coactivators CBP/EP300 facilitate cellular reprogramming. Nat. Chem. Biol. *15*, 519–528.
34. de Pooter, R.F., and Kee, B.L. (2010). E proteins and the regulation of early lymphocyte development. Immunol. Rev. *238*, 93–109.
35. Raisner, R., Kharbanda, S., Jin, L., Jeng, E., Chan, E., Merchant, M., Haverty, P.M., Bainer, R., Cheung, T., Arnott, D., et al. (2018). Enhancer Activity Requires CBP/P300 Bromodomain-Dependent Histone H3K27 Acetylation. Cell Rep. *24*, 1722–1729.
36. Largeot, A., Perez-Campo, F.M., Marinopoulou, E., Lie-a-Ling, M., Kouskoff, V., and Lacaud, G. (2016). Expression of the MOZ-TIF2 oncoprotein in mice represses senescence. Exp. Hematol. *44*, 231–237.e4.
37. Lin, C.H., Wang, Z., Duque-Afonso, J., Wong, S.H.K., Demeter, J., Loktev, A.V., Somervaille, T.C.P., Jackson, P.K., and Cleary, M.L. (2019). Oligomeric self-association contributes to E2A-PBX1-mediated oncogenesis. Sci. Rep. *9*, 4915.
38. Karasuyama, H., and Melchers, F. (1988). Establishment of mouse cell lines which constitutively secrete large quantities of interleukin 2, 3, 4 or 5, using modified cDNA expression vectors. Eur. J. Immunol. *18*, 97–104.
39. Harris, W.J., Huang, X., Lynch, J.T., Spencer, G.J., Hitchin, J.R., Li, Y., Ciceri, F., Blaser, J.G., Greystoke, B.F., Jordan, A.M., et al. (2012). The histone demethylase KDM1A sustains the oncogenic potential of MLL-AF9 leukemia stem cells. Cancer Cell *21*, 473–487.
40. Van Gosliga, D., Schepers, H., Rizo, A., van der Kolk, D., Vellenga, E., and Schuringa, J.J. (2007). Establishing long-term cultures with self-renewing

acute myeloid leukemia stem/progenitor cells. Exp. Hematol. *35*, 1538–1549.

41. Somervaille, T.C.P., Linch, D.C., and Khwaja, A. (2003). Different levels of p38 MAP kinase activity mediate distinct biological effects in primary human erythroid progenitors. Br. J. Haematol. *120*, 876–886.
42. Dobin, A., Davis, C.A., Schlesinger, F., Drenkow, J., Zaleski, C., Jha, S., Batut, P., Chaisson, M., and Gingeras, T.R. (2013). STAR: ultrafast universal RNA-seq aligner. Bioinformatics *29*, 15–21.
43. Love, M.I., Huber, W., and Anders, S. (2014). Moderated estimation of fold change and dispersion for RNA-seq data with DESeq2. Genome Biol. *15*, 550.
44. Hafemeister, C., and Satija, R. (2019). Normalization and variance stabilization of single-cell RNA-seq data using regularized negative binomial regression. Genome Biol. *20*, 296.
45. Satija, R., Farrell, J.A., Gennert, D., Schier, A.F., and Regev, A. (2015). Spatial reconstruction of single-cell gene expression data. Nat. Biotechnol. *33*, 495–502.
46. Waltman, L., and van Eck, N.J. (2013). A smart local moving algorithm for large-scale modularity-based community detection. Eur. Phys. J. B *86*, 471.
47. Granja, J.M., Klemm, S., McGinnis, L.M., Kathiria, A.S., Mezger, A., Corces, M.R., Parks, B., Gars, E., Liedtke, M., Zheng, G.X.Y., et al. (2019). Single-cell multiomic analysis identifies regulatory programs in mixed-phenotype acute leukemia. Nat. Biotechnol. *37*, 1458–1465.
48. Hie, B., Bryson, B., and Berger, B. (2019). Efficient integration of heterogeneous single-cell transcriptomes using Scanorama. Nat. Biotechnol. *37*, 685–691.
49. Lee, T.I., Johnstone, S.E., and Young, R.A. (2006). Chromatin immunoprecipitation and microarray-based analysis of protein location. Nat. Protoc. *1*, 729–748.
50. Zhang, Y., Liu, T., Meyer, C.A., Eeckhoute, J., Johnson, D.S., Bernstein, B.E., Nusbaum, C., Myers, R.M., Brown, M., Li, W., and Liu, X.S. (2008). Model-based analysis of ChIP-Seq (MACS). Genome Biol. *9*, R137.
51. Heinz, S., Benner, C., Spann, N., Bertolino, E., Lin, Y.C., Laslo, P., Cheng, J.X., Murre, C., Singh, H., and Glass, C.K. (2010). Simple combinations of lineage-determining transcription factors prime cis-regulatory elements required for macrophage and B cell identities. Mol. Cell *38*, 576–589.
52. Lawrence, M., Huber, W., Pagès, H., Aboyoun, P., Carlson, M., Gentleman, R., Morgan, M.T., and Carey, V.J. (2013). Software for Computing and Annotating Genomic Ranges. PLoS Comput. Biol. *9*, e1003118.
53. Buenrostro, J.D., Giresi, P.G., Zaba, L.C., Chang, H.Y., and Greenleaf, W.J. (2013). Transposition of native chromatin for fast and sensitive epigenomic profiling of open chromatin, DNA-binding proteins and nucleosome position. Nat. Methods *10*, 1213–1218.
54. Andrews, S. (2010). FastQC: a quality control tool for high throughput sequence data. http://www.bioinformatics.babraham.ac.uk/projects/fastqc.
55. Martin, M. (2011). Cutadapt removes adapter sequences from high-throughput sequencing reads. EMBnet. j. *17*, 10–12.
56. Li, H., and Durbin, R. (2009). Fast and accurate short read alignment with Burrows-Wheeler transform. Bioinformatics *25*, 1754–1760.
57. Li, H., Handsaker, B., Wysoker, A., Fennell, T., Ruan, J., Homer, N., Marth, G., Abecasis, G., and Durbin, R.; 1000 Genome Project Data Processing Subgroup (2009). The Sequence Alignment/Map format and SAMtools. Bioinformatics *25*, 2078–2079.
58. Fabian, M.A., Biggs, W.H., Treiber, D.K., Atteridge, C.E., Azimioara, M.D., Benedetti, M.G., Carter, T.A., Ciceri, P., Edeen, P.T., Floyd, M., et al. (2005). A small molecule-kinase interaction map for clinical kinase inhibitors. Nat. Biotechnol. *23*, 329–336.
59. Subramanian, A., Tamayo, P., Mootha, V.K., Mukherjee, S., Ebert, B.L., Gillette, M.A., Paulovich, A., Pomeroy, S.L., Golub, T.R., Lander, E.S., and Mesirov, J.P. (2005). Gene set enrichment analysis: a knowledge-based approach for interpreting genome-wide expression profiles. Proc. Natl. Acad. Sci. USA *102*, 15545–15550.

STAR★METHODS

KEY RESOURCES TABLE

REAGENT or RESOURCE	SOURCE	IDENTIFIER
Antibodies		
anti-acetyl H3K9	Abcam	Cat# ab4441; RRID: AB_2118292
anti-acetyl H3K18	Cell Signaling Technology	Cat# 9675; RRID: AB_331550
anti-acetyl H3K27	Abcam	Cat# ab4729; RRID: AB_2118291
anti-Histone H3	Cell Signaling Technology	Cat# 3638; RRID: AB_1642229
anti-acetyl H4K5	Cell Signaling Technology	Cat# 8647; RRID: AB_11217428
anti-Histone H4	Cell Signaling Technology	Cat# 2935; RRID: AB_1147658
anti-α Tubulin	This study	In house
anti-EP300	Active Motif	Cat# 61401; RRID: AB_2716754
anti-MYB	Millipore	Cat# 05-175; RRID: AB_11213983
anti-CEBPA	Diagenode	Cat# C15410225; RRID: AB_2737367
anti-SPI1	Cell Signaling Technology	Cat# 2258; RRID: AB_2186909
anti-RUNX1	Abcam	Cat# ab23980; RRID:AB_2184205
anti-IRF4	Cell Signaling Technology	Cat# 4964; RRID:AB_10698467
anti-TCF3/E2A	Cell Signaling Technology	Cat# 12258; RRID: AB_2797860
anti-RFX5	Rockland	Cat# 200-401-194; RRID: AB_2253725
anti-FLI1	Abcam	Cat# ab133485; RRID: AB_2722650
anti-ETV6	Atlas Antibodies	Cat# HPA000264; RRID: AB_611466
anti-ELF1	Santa Cruz Biotechnology	Cat# sc-133096; RRID: AB_2262155
anti-Vinculin	Sigma-Aldrich	Cat# V9131; RRID: AB_477629
anti-MYB	Abcam	Cat# ab45150; RRID: AB_778878
anti-RNA polymerase II	Abcam	Cat# ab26721; RRID: AB_777726
anti-RNA polymerase II (phospho S2)	Abcam	Cat# ab5095; RRID:AB_304749
anti-RNA polymerase II (phospho S5)	Abcam	Cat# ab5408; RRID: AB_304868
anti-CREBBP	Abcam	Cat# ab253202; RRID:AB_2939015
anti-EP300	Bio-Rad	Cat# MCA6390; RRID: AB_2939018

(*Continued on next page*)

Continued

REAGENT or RESOURCE	SOURCE	IDENTIFIER
Goat anti-Rabbit IgG (H+L) Cross-Adsorbed Secondary Antibody, HRP	ThermoFisher	Cat# 31462; RRID: AB_228338
Amersham ECL Mouse IgG, HRP-linked whole Ab (from sheep)	Cytiva	Cat# NA931; RRID:AB_772210
anti-CD86-PerCP-eFlour710	ThermoFisher	Cat# 46086282; RRID: AB_2815140
Anti-CD11b-PE	BD Pharmingen	Cat# 555388; RRID: AB_395789
Anti-Mac1 PE	Invitrogen	Cat# 12-0112-82; RRID: AB_2734869
Anti-GR1 PE-CY7	Invitrogen	Cat# 25-5931-82; RRID: AB_469663
Anti-CD117-APC	Invitrogen	Cat# 17-1171-83; RRID: AB_469431
Anti-TCRβ-APC-eF780	Invitrogen	Cat# 47-5961-80; RRID: AB_1272209
Anti-B220-eF450	Invitrogen	Cat# 48-0452-80; RRID: AB_1548763
Bacterial and virus strains		
One shot Stbl3 Chemically Competent E.Coli	ThermoFisher	Cat# C737303
DH5a Chemically Competent E.Coli	ThermoFisher	Cat# 18265017
Stellar™ Competent Cells	TAKARA BIO	Cat# 636766
Biological samples		
Primary human AML samples	Manchester Cancer Research Centre Tissue Biobank	the-christie.biobank@nhs.net
Chemicals, peptides, and recombinant proteins		
Puromycin	Sigma	Cat# P8833
β-Mercaptoethanol	Sigma	Cat# M3148
Hydrocortisone	Sigma	Cat# H0135
Minimum Eagles Medium – Alpha modification	Gibco	Cat# 12561-056
Dulbecco's Modified Eagles Medium	Sigma	Cat# D6546
RPMI-1640 medium	Sigma	Cat# R0883
RPMI-1640 medium phenol red free	Sigma	Cat# R7509
Foetal Bovine Serum	Sigma	Cat# F7524
Heat inactivated Foetal Bovine Serum	Gibco	Cat# 10500064
Heat inactivated Horse Serum	Gibco	Cat# 26050-088
Trypsin EDTA	Sigma	Cat# T3924
L-glutamine	Sigma	Cat# G7513
Penicillin/Streptomycin	Sigma	Cat# P0781
Human recombinant IL3	Peprotech	Cat# 200-03
Human recombinant GCSF	Peprotech	Cat# 300-23
Human recombinant TPO	Peprotech	Cat# 300-18
Murine recombinant IL3	Peprotech	Cat# 213-13
Murine recombinant GM-CSF	Peprotech	Cat# 315-03
Murine recombinant SCF	Peprotech	Cat# 250-03
Murine recombinant IL-6	Peprotech	Cat# 216-16
Venetoclax	Selleck Chemicals	Cat# S8048
Bortezomib	Meilun Biotech	Cat# MB1040-2
Lenalidomide	Meilun Biotech	Cat# MB1136-1
Cytarabine	MedChemExpress	Cat# HY-13605
Azacytidine	Sigma	Cat# A2385

(*Continued on next page*)

Continued

REAGENT or RESOURCE	SOURCE	IDENTIFIER
Vorinostat	Meilun Biotech	Cat# MB1265-1
Human MethoCult	Stem Cell Technologies	Cat# 04230
Mouse MethoCult	Stem Cell Technologies	Cat# M3231
Resazurin Sodium Salt	Sigma	Cat# R7017
Dynabeads Protein G	Invitrogen	Cat# 10004D
T4 DNA Ligase	NEB	Cat# M0202L
T4 DNA Ligase	Roche	Cat# 799009
Polybrene	Milipore	Cat# TR1003G
Trypan Blue Solution	GIBCO	Cat# 15250-061
Formaldehyde	Sigma-Aldrich	Cat# F8775
ChIP cross-link Gold	Diagenode	Cat# C01019027
SYBR Green PCR Master Mix	ThermoFisher	Cat# 4309155
May-Grunwald Giemsa	Sigma	Cat# MG500
cOmplete EDTA-free Protease Inhibitor Cocktail	Roche	Cat# 11873580001
Benzonase Nuclease	Millipore	Cat# E1014
NuPAGE LDS Sample Buffer	Invitrogen	Cat# NP0007
NUPAGE 4-12% Bis-Tris GEL 1.0MM10W	Invitrogen	Cat# NP0321BOX
NUPAGE 4-12% Bis-Tris GEL 1.0MM12W	Invitrogen	Cat# NP0322BOX
Bovine Serum Albumin	Sigma-Aldrich	Cat# A4503
TWEEN20	Sigma-Aldrich	Cat# P1379
Amersham Protran Supported 0.2um NC 300mm x 4m roll	Cytiva	Cat# 10600015
Clarity Western ECL Substrate	Bio-Rad	Cat# 1705060
SuperSignal West Femto Maximum Sensitivity Substrate	ThermoFisher	Cat# 34095
Restore Western Blot Stripping Buffer	ThermoFisher	Cat# 21059
TaqMan Gene Expression Assay (FAM) Primer-probe mix	ThermoFisher	Cat# 4331182
TaqMan Fast Universal PCR Master Mix (2X)	ThermoFisher	Cat# 4367846
RNAlater Solutions for RNA Stabilization and Storage	ThermoFisher	Cat# AM7020
RNAse A	Roche	Cat# 10109169001
Recombinant Proteinase K Solution	ThermoFisher	Cat# AM2546
Phenol:Chloroform:Isoamyl Alcohol 25:24:1	Sigma-Aldrich	Cat# P2069
Chloroform:Isoamyl alcohol 24:1	Sigma-Aldrich	Cat# C0549
Glycogen	Roche	Cat# 10901393001
AMPure XP Reagent	Beckman Coulter	Cat# A63881
Tagmentase (Tn5 transposase) - loaded	Diagenode	Cat# C01070012
Tagmentation Buffer (2x)	Diagenode	Cat# C01019043
NEBNext High-Fidelity 2X PCR Master Mix	NEB	Cat# M0541
CCS1477	CellCentric	N/A
DIMETHYL SULFOXIDE (DMSO)	VWR Chemicals	Cat# 0231
Cycloheximide (CHX)	Sigma-Aldrich	Cat# 01810
MG-132	Sigma-Aldrich	Cat# M7449
Propidium iodide solution	Sigma-Aldrich	Cat# P4864
SYBR Green I Nucleic Acid Gel Stain	ThermoFisher	Cat# S7563
NdeI	NEB	Cat# R0111L
NheI HF	NEB	Cat# R3131L
AgeI HF	NEB	Cat# R3552L
EcoRI HF	NEB	Cat# R3101L
Critical commercial assays		
RNeasy Plus Micro Kit	QIAGEN	Cat# 74034
RNeasy Plus Mini Kit	QIAGEN	Cat# 74134
High-Capacity cDNA Reverse Transcription	ThermoFisher	Cat# 4368814

(*Continued on next page*)

Continued

REAGENT or RESOURCE	SOURCE	IDENTIFIER
APC Annexin Kit	BD Pharmigen	Cat# 550474
DNeasy blood and tissue kit	QIAGEN	Cat# 69504
QIAamp DNA Blood Mini Kit	QIAGEN	Cat# 51104
QIAshredder	QIAGEN	Cat# 79656
QIAquick PCR Purification Kit	QIAGEN	Cat# 28104
MinElute PCR Purification Kit	QIAGEN	Cat# 28004
Pierce BCA protein assay Kit	ThermoFisher	Cat# 23225
Subcellular Protein Fractionation Kit for Cultured Cells	ThermoFisher	Cat# 78840
Microplex Library Preparation Kit	Diagenode	Cat# C05010012
NEB Next Ultra II DNA Library Prep Kit for Illumina	NEB	Cat# E7645S
NEBNext Ultra II Directional RNA Library Prep Kit for Illumina	NEB	Cat# E7760
NEBNext rRNA Depletion Kit v2 (Human/Mouse/Rat) with RNA Sample Purification Beads	NEB	Cat# E7405
KAPA RNA HyperPrep Kit with RiboErase (HMR)	Roche	Cat# KK8560
Chromium Next GEM Single Cell 3' Reagent Kit v3.1	10x Genomics	Cat# PN-1000121
SureSelect Strand - Specific RNA Library Preparation kit for Illumina	Agilent	Cat# G9691A
Kapa Library Quantification Kit for Illumina sequencing	Roche	Cat# 07960140001
Deposited data		
TS50_3_DMSO_3_SPI1_S3	Maiques-Diaz et al.[13]	GSM3057096
TS120_RUNX1_NTC	Simeoni et al.[14]	GSM4837708
ENCSR000EGO	ENCODE Project Consortium et al.[15]	GSM935565
DNA and RNA sequencing data produced in this study	This study	GEO: GSE207357
TS163_01_6h_DMSO_rep1	This study	GSM6284883
TS163_02_6h_CCS1477_100nM_rep2	This study	GSM6284884
TS163_03_6h_DMSO_rep2	This study	GSM6284885
TS163_04_6h_CCS1477_100nM_rep1	This study	GSM6284886
TS181_07_48hDMSOREP2_S7	This study	GSM7441201
TS181_08_48hCCS1477REP2_S8	This study	GSM7441202
TS181_09_48hDMSOREP1_S9	This study	GSM7441203
TS181_10_48hCCS1477REP1_S10	This study	GSM7441204
TS50_5_DMSO_5_CEBP_a	This study	GSM6284887
TS162_05_H3K27ac-CCS1477_6h_100nM	This study	GSM6284890
TS162_09_H3K27ac-DMSO_6h	This study	GSM6284891
TS162_10_Input-THP1	This study	GSM6284892
phosphoS2Pol2CCS1477_6h_100nM	This study	GSM6284893
phosphoS2Pol2DMSO_6h	This study	GSM6284894
phosphoS5Pol2CCS1477_6h_100nM	This study	GSM6284895
phosphoS5Pol2DMSO_6h	This study	GSM6284896
Pol2CCS1477_6h_100nM	This study	GSM6284897
Pol2DMSO_6h	This study	GSM6284898
TS171_01_THP1_p300_48h_CCS1477_100nM	This study	GSM6284899
TS171_02_THP1_p300_6h_CCS1477_100nM	This study	GSM6284900
TS171_03_THP1_p300_6h_DMSO	This study	GSM6284901
TS171_04_THP1_p300_48h_DMSO	This study	GSM6284902
TS172_01_OPM2_p300_48h_DMSO	This study	GSM6284903
TS172_02_OPM2_p300_48h_CCS1477_100nM	This study	GSM6284904
TS172_03_OPM2_INPUT	This study	GSM6284905
TS172_04_OPM2_p300_6h_DMSO	This study	GSM6284906
TS172_05_OPM2_p300_6h_CCS1477_100nM	This study	GSM6284907

(*Continued on next page*)

Continued

REAGENT or RESOURCE	SOURCE	IDENTIFIER
TS179_01_p300_1h_CCS1477_S13	This study	GSM7441260
TS179_02_MYB_1h_CCS1477_S14	This study	GSM7441261
TS179_03_p300_2h_CCS1477_S15	This study	GSM7441262
TS179_04_MYB_2h_DMSO_S16	This study	GSM7441263
TS179_05_MYB_6h_CCS1477_S17	This study	GSM7441264
TS179_06_MYB_1h_DMSO_S18	This study	GSM7441265
TS179_07_MYB_6h_DMSO_S19	This study	GSM7441266
TS179_09_MYB_2h_CCS1477_S21	This study	GSM7441267
TS179_11_p300_1h_DMSO_S23	This study	GSM7441268
TS179_14_p300_2h_DMSO_S26	This study	GSM7441269
TS180_01_IRF4_6h_CCS1477_OPM2_S1	This study	GSM7441270
TS180_02_IRF4_6h_DMSO_OPM2_S2	This study	GSM7441271
TS180_03_IRF4_48h_DMSO_OPM2_S3	This study	GSM7441272
TS180_04_IRF4_48h_CCS1477_OPM2_S4	This study	GSM7441273
TS181_01_OPM2CBP48hDMSO_S1	This study	GSM7441274
TS181_02_OPM2CBP48hCCS1477_S2	This study	GSM7441275
TS181_03_THP1CBP6hCCS1477_S3	This study	GSM7441276
TS181_04_OPM2CBP6hCCS1477_S4	This study	GSM7441277
TS181_05_THP1CBP6hDMSO_S5	This study	GSM7441278
TS181_06_OPM2CBP6hDMSO_S6	This study	GSM7441279
TS183_02_p300_48h_CCS1477_1000nM_S2	This study	GSM7441280
TS183_04_p300_48h_DMSO_1000nM_S4	This study	GSM7441281
TS183_05_p300_6h_DMSO_1000nM_S5	This study	GSM7441282
TS183_07_p300_6h_CCS1477_1000nM_S7	This study	GSM7441283
TS186_05_shx_H3K27ac_THP1_S5	This study	GSM7506239
TS186_07_MYB_KD6_H3K27ac_THP1_S7	This study	GSM7506240
TS184_01_E2A_48h_DMSO_OPM-2_S9	This study	GSM7441284
TS184_02_E2A_6h_DMSO_OPM-2_S10	This study	GSM7441285
TS184_03_RUNX1_48h_CCS1477_OPM-2_S11	This study	GSM7441286
TS184_04_RUNX1_48h_DMSO_OPM-2_S12	This study	GSM7441287
TS184_05_RUNX1_6h_CCS1477_OPM-2_S13	This study	GSM7441288
TS184_06_RUNX1_6h_DMSO_OPM-2_S14	This study	GSM7441289
TS184_07_E2A_6h_CCS1477_OPM-2_S15	This study	GSM7441290
TS184_08_E2A_48h_CCS1477_OPM-2_S16	This study	GSM7441291
TS186_01_H3K27ac_6h_DMSO_OPM-2_S1	This study	GSM7441292
TS186_02_MYB_48h_DMSO_OPM-2_S2	This study	GSM7441293
TS186_03_H3K27ac_6h_CCS1477_OPM-2_S3	This study	GSM7441294
TS186_04_H3K27ac_48h_DMSO_OPM-2_S4	This study	GSM7441295
TS186_06_MYB_6h_DMSO_OPM-2_S6	This study	GSM7441296
TS186_09_MYB_6h_CCS1477_OPM-2_S9	This study	GSM7441297
TS186_10_MYB_48h_CCS1477_OPM-2_S10	This study	GSM7441298
TS186_11_H3K27ac_48h_CCS1477_OPM-2_S11	This study	GSM7441299
TS169_05_THP1_CCS1477_6h_100nM	This study	GSM6284908
TS169_06_THP1_DMSO_48h	This study	GSM6284909
TS169_07_THP1_DMSO_6h	This study	GSM6284910
TS169_08_THP1_CCS1477_48h_100nM	This study	GSM6284911
TS185_01_OPM-2_DMSO_6h_S1	This study	GSM7441300
TS185_02_OPM-2_CCS1477_6h_S2	This study	GSM7441301
TS185_03_OPM-2_DMSO_48h_S3	This study	GSM7441302
TS185_04_OPM-2_CCS1477_48h_S4	This study	GSM7441303

(*Continued on next page*)

Continued

REAGENT or RESOURCE	SOURCE	IDENTIFIER
D5_veh_S2071_00001	This study	GSM7506252
D5_veh_S2071_00002	This study	GSM7506253
D5_veh_S2071_00003	This study	GSM7506254
D5_veh_S2071_00004	This study	GSM7506255
CCS20_D5_S2071_00009	This study	GSM7506256
CCS20_D5_S2071_00010	This study	GSM7506257
CCS20_D5_S2071_00011	This study	GSM7506258
CCS20_D5_S2071_00012	This study	GSM7506259
TS173_04_Sample_D_screening_pretreatment	This study	GSM6284912
TS173_05_Sample_E_treatment_timepoint2_Cycle2_Day3	This study	GSM6284913
TS173_06_Sample_F_treatment_timepoint4_Cycle4_Day1	This study	GSM6284914
Experimental models: Cell lines		
THP1 (M)	DSMZ	RRID:CVCL_0006
HEK293 (F)	Invitrogen	RRID:CVCL_0045
OPM2 (F)	DSMZ	RRID:CVCL 1625
X63Ag8-653 (F)	DSMZ	RRID:CVCL 4032
ATN-1 (M)	RIKEN	RRID:CVCL_1073
CCRF-CEM (F)	ATCC	RRID:CVCL_0207
CTB-1 (M)	RIKEN	RRID:CVCL_1149
EB1 (F)	ATCC	RRID:CVCL_2027
GA-10 (M)	ATCC	RRID:CVCL_1222
HEL (M)	HSRRB	RRID:CVCL_0001
HEL92.1.7 (M)	ATCC	RRID:CVCL_2481
HL-60 (F)	ATCC	RRID:CVCL_0002
IM-9 (F)	HSRRB	RRID:CVCL_1305
JeKo-1 (F)	ATCC	RRID:CVCL_1865
Jurkat (M)	ATCC	RRID:CVCL_0065
KG-1 (M)	ATCC	RRID:CVCL_0374
KMS.11 (F)	HSRRB	RRID:CVCL_2989
KMS.12-PE (F)	DSMZ	RRID:CVCL_1333
KMS.28BM (F)	HSRRB	RRID:CVCL_2994
KMS-20 (F)	HSRRB	RRID:CVCL_2990
Loucy (F)	ATCC	RRID:CVCL_1380
LP-1 (F)	DSMZ	RRID:CVCL_0012
MAVER-1 (M)	ATCC	RRID:CVCL_1831
MLMA (F)	HSRRB	RRID:CVCL_1419
MM.1R (F)	ATCC	RRID:CVCL_8794
MOLM16 (F)	DSMZ	RRID:CVCL_2120
MOLT-4 (M)	NCI	RRID:CVCL_0013
NAMALWA (M)	ATCC	RRID:CVCL_0067
NOMO-1 (F)	HSRRB	RRID:CVCL_1609
OCI-AML-3 (M)	DSMZ	RRID:CVCL_1844
OPM-2 (F)	DSMZ	RRID:CVCL_1625
OPM-2_LenR (F)	This study	N/A
P116 (M)	ATCC	RRID:CVCL_6429
Pfeiffer (M)	ATCC	RRID:CVCL_3326
Raji (M)	ATCC	RRID:CVCL_0511
REH (F)	ATCC	RRID:CVCL_1650
RPMI8226 (M)	ATCC	RRID:CVCL_0014

(*Continued on next page*)

Continued

REAGENT or RESOURCE	SOURCE	IDENTIFIER
SUP.T1 (M)	ATCC	RRID:CVCL_1714
THP-1 (M)	ATCC	RRID:CVCL_0006
U266B1 (M)	ATCC	RRID:CVCL_0566
MLL-AF9 mouse cells (M and F)	Generated in house	N/A
MLL-ENL mouse cells (M and F)	Generated in house	N/A
E2A-PBX1 mouse cells (M and F)	Generated in house	N/A
MOZ-TIF2 mouse cells (M and F)	Gift from G Lacaud	N/A
Oligonucleotides		
See Table S4	This study	N/A
Recombinant DNA		
pLKO.1 - TRC cloning vector	Addgene	Cat# 10878, RRID:Addgene_10878
pLKO.1 (SHC002): NTC	Sigma Aldrich	Cat# SHC002
pLKO.1: MYB KD	This study	N/A
pLKO.1: IRF4 KD1	This study	N/A
pLKO.1: IRF4 KD2	This study	N/A
EF1α_MCS_SV40_puro	Generated in house	N/A
pCMVR8.74	Addgene	Cat# #22036 RRID:Addgene_22036
pMD2.G	Addgene	Cat# #12259 RRID:Addgene_12259
Software and algorithms		
STAR v2.4.2a	Dobin et al.[42]	N/A
BWA-MEM v0.7.15	Li et al.[56]	N/A
Cell Ranger v5.0.1	10x Genomics Cell Ranger 5.0.1	N/A
Seurat package	Satija et al.[45]	N/A
Louvain algorithm	Waltman et al.[46]	N/A
Scanorama	Hie et al.[48]	N/A
Samtools v0.1.9	Li et al.[57]	N/A
MACS2	Zhang et al.[50]	N/A
Homer v4.10	Heinz et al.[51]	N/A
GenomicRanges v1.30.1	Lawrence et al.[52]	N/A
FASTQC v0.11.3	Andrews et al.[54]	N/A
Cutadapt	Martin et al.[55]	N/A
DESeq2	Love et al.[43]	N/A
SDS software v2.1	Applied Biosystems	N/A
GSEA v2.0.14	Subramanian et al.[59]	N/A
Microsoft Excel 2016	N/A	N/A
StatsDirect software v.1.9.7	StatsDirect	N/A
GREAT	Liberzon et al.[18]	N/A
MEME-ChIP	Machanick et.[11]	N/A

RESOURCE AVAILABILITY

Lead contact

Further information and requests for resources and reagents should be directed to and will be fulfilled by the lead contact, Tim Somervaille (tim.somervaille@cruk.manchester.ac.uk).

Materials availability

- This study did not generate new unique reagents.
- All plasmids listed in the key resources table are available upon request.

Data and code availability

- ChIPseq and RNAseq data have been deposited at GEO and are publicly available as of the date of publication. Accession numbers are listed in the key resources table.
- This paper does not report original code.
- Any additional information required to reanalyze the data reported in this paper is available from the lead contact on request.
- The accession number for high-throughput sequencing data files reported in this paper is GSE207357.

EXPERIMENTAL MODEL AND STUDY PARTICIPANT DETAILS

Animal studies

Transplantation experiments using mice were approved by the Animal Welfare and Ethics Review Body at Cancer Research UK Manchester Institute and performed under a project license issued by the United Kingdom Home Office, in keeping with the Home Office Animal Scientific Procedures Act of 1986. Cryopreserved female bone marrow cells from female mice with experimentally initiated AML (retroviral transduction and transplantation of KIT+ BM stem and progenitor cells)[27] were thawed and cultured for seven days before $1x10^6$ MLL-AF9 or MLL-AF10 AML cells were injected into the tail veins of sub-lethally irradiated (2 x 200cGy) female recipient C57BL/6 mice which were 8-10 weeks old (Harlan, Huntingdon, UK). Cells were allowed to engraft for two weeks following which mice were dosed with CCS1477 (30mg/kg) or DMSO containing vehicle by oral gavage daily for 42 days. Transplanted mice exhibiting signs of ill health, or healthy mice at the end of the study (Day 220), were euthanized using a Schedule 1 method. Cells from BM were cryopreserved for later analysis. In preparation of figures, no animals were excluded.

In vivo xenograft studies were performed by Crown Bioscience (Beijing, People's Republic of China). Animals were housed in pathogen-free facilities and all studies were reviewed and approved ahead of time by Crown Bioscience's Institutional Animal Care and Use Committee (IACUC). During the study, the care and use of animals was conducted in accordance with the regulations of the Association for Assessment and Accreditation of Laboratory Animal Care (AAALAC). Xenograft tumours were established by subcutaneous injection of MOLM16, OPM-2 or MV(4,11) cells into female 7-10 week old NOD.CB17-Prkdc^{scid} (NOD/SCID) mice sourced from AK Bioscience C., Ltd (Beijing, People's Republic of China). Once tumours had reached approximately $150mm^3$, animals were randomized into control and treated groups. CCS1477 was administered by oral gavage once daily. In all studies, tumour volume (measured by calliper), animal body weight, and condition were monitored at least twice weekly. At various time points, blood (for serum or plasma) and tumour samples were collected for bioanalysis of CCS1477 concentrations and analysis of pharmacodynamic (PD) biomarkers. In preparation of figures, no animals were excluded.

Assessment of normal hematopoiesis in rats treated with CCS1477 was performed by Sequani Limited (Ledbury, UK) under authority of a Project Licence in compliance with the Animals (Scientific Procedures) Act 1986. Male Crl:WI(Han) rats were dosed with 0 (vehicle) or 7.5 mg/kg/day CCS1477 once daily (n=6 per cohort). The vehicle consisted of 5% v/v DMSO, 5% v/v Ethanol and 18% w/v Vitamin E D-a-tocopheryl polyethylene glycol succinate (TPGS) in ultra-high purity water. Both groups were dosed by gavage at a dose volume of 5 mL/kg for 14 days. All animals were assessed for clinical observations, body weights and food intake. Blood samples were taken during the acclimatisation period, and on days 7 and 14 of dosing. There were no deaths during the study and no clinical signs of toxicity. In preparation of figures, no animals were excluded.

For clonogenic assays of murine (M3231, Stem Cell Technologies) AML cells, cells were cultured at $2.5x10^3$ cells/ml in methylcellulose medium supplemented with IL3, IL6, GM-CSF (10ng/ml) and SCF (20ng/ml). Colonies were enumerated after 5-10 days in culture.

Murine MLL-AF9, MLL-ENL, E2A-PBX1 leukemias or MOZ-TIF2 immortalized cells were generated by retroviral transduction and/or transplantation as described.[27,36,37] Cryopreserved leukemia cells from these previously published cohorts were thawed and then cultured in RPMI with 10% FBS and 10% X-63 conditioned medium[38] supplemented with 2mM L-glutamine.

Human participants

Human participants were treated on CCS1477-02 which is an ongoing multi-centre, open-label, non-randomized, multicohort, phase I/IIa study (ClinicalTrials.gov identifier: NCT04068597) in which subjects with a range of advanced hematological malignancies are treated with CCS1477 (Data S1 and S2). During the Phase I monotherapy dose escalation portion of this study, CCS1477 was administered in 28-day cycles at doses ranging from 25-50mg once or twice daily in a continuous or intermittent schedule. The study and all associated documentation received ethical approval from South Central Berkshire Research Ethics Committee (Reference 19/SC/0221). The study was conducted in accordance with the study protocol, local guidelines and regulations, and in keeping with the ethical principles of the Declaration of Helsinki. All patients gave their written informed consent ahead of participation. Treatment was continued until disease progression, unacceptable toxicity or consent withdrawal.

Eligible patients were over 18 years of age, male or female. Patients had confirmed (as per standard disease specific diagnostic criteria) relapsed or refractory AML or myeloma and had exhausted appropriate standard-of-care treatment options. Patients had to have adequate hematologic function (unless the diagnosis was AML) which was defined as an absolute neutrophil count of ≥ 1.0 x 10^9/L, platelet count ≥ 75 x 10^9/L and hemoglobin level ≥ 80 g/L. For AML, the WBC had to be <10 x 10^9/L. All patients had to have an Eastern Cooperative Oncology Group performance status of ≤ 2 and adequate organ function, defined as defined as: serum aspartate aminotransferase (AST) and alanine aminotransferase (ALT) ≤ 3 x upper limit of normal (ULN), or AST/ALT ≤ 5 x ULN, total

bilirubin $\leq$1.5 x ULN; creatinine clearance $\geq$50 mL/min and serum albumin >2.5 g/dL. Safety evaluations were performed throughout the study.

Here we report exemplar cases treated since March 2021 from three centers in the United Kingdom to illustrate how the *in vitro* and *in vivo* pre-clinical activity of CCS1477 extends into patients; a full trial report will be published separately in due course.

Cell lines

Cell lines (see key resources table) were cultured in RPMI 1640, alpha-MEM or IMDM containing 10-20% fetal bovine serum (FBS), varying according to the recommendations of ATCC or DMSZ. Where possible cell line authentication was performed by STR analysis. Cell line sex is shown in the key resources table.

For growth assays, cells were exposed in duplicate or quintuplicate to a nine-point dosing with CCS1477 (top dose 10μM). The effects of CCS1477 were evaluated using CellTiter-Glo (Promega, Madison, WI) or alamarBlue (ThermoFisher, Waltham, MA), according to the manufacturer's instructions. For semisolid clonogenic assays, human AML cells were cultured at a density of $1x10^4$ cells/ml in methylcellulose medium (H4320, Stem Cell Technologies).

To generate FUCCI THP1 AML cells, the coding sequences for the two FUCCI fluorescent fusion proteins mKO2-CDT1 and mAG-GMNN were PCR amplified from commercially available plasmid templates (Amalgaam, Japan) and cloned into an EF1α_MCS_SV40_puro lentiviral plasmid using NdeI and NheI restriction endonucleases. Lentivirus was generated in 293FT cells (ThermoFisher) as described[14,39] and THP1 cells transduced with lentiviral particles in the presence of 8μg/ml polybrene. To isolate a single clone of THP1 cells expressing both the CDT1 and GMNN FUCCI constructs sequentially as cells moved through the cycle, cells were plated in semisolid culture at low density following infection with both lentiviruses and then single colonies containing a mixture of red and green cells were plucked from the medium and expanded.

Primary cells

Use of primary human tissue was in compliance with the ethical and legal framework of the UK's Human Tissue Act, 2004. Primary human AML samples were from Manchester Cancer Research Centre's Tissue Biobank (instituted with the approval of the South Manchester Research Ethics Committee (18/NW/0092) and licensed by the Human Tissue Authority (licence number: 30004)). Their use was authorized following ethical review by the Tissue Biobank's scientific sub-committee (approval reference 08_TISO-02) and with the informed consent of the donor. Donor sex and age are shown in Table S2.

Cryopreserved primary patient AML samples from blood or bone marrow were thawed and recovered on MS5 stromal cells for 7-10 days in alpha-MEM medium supplemented with 12.5% heat-inactivated FBS, 12.5% heat-inactivated horse serum, 2mM L-glutamine, 57.2μM β-mercaptoethanol, 1 μM hydrocortisone and 20 ng/ml IL3, G-CSF and TPO (Peprotech, London, UK), as described.[40] Primary AML cells for growth assays using alamarBlue were then switched to liquid culture in StemSpan (Stem Cell Technologies, Vancouver, Canada) supplemented with IL3, G-CSF and TPO (all at 20ng/ml) (Peprotech, London, UK). Cell cycle, apoptosis and differentiation assays of primary AML cells were performed in stromal coculture.

For clonogenic assays of human primary AML cells, cells were cultured at $2x10^4$ cells/ml in methylcellulose medium supplemented with IL3, G-CSF and TPO (20ng/ml). Colonies were enumerated after 5-10 days in culture.

METHOD DETAILS

Flow cytometry, apoptosis and cell cycle analysis

Flow cytometric analyses were performed using an LSR Model II flow cytometer (BD Biosciences, Oxford, UK) using the following antibodies: CD11b PE (ICRF44), CD86 PerCP-EF710 (B7-2), CD11b-PE (M-170), Ly-6G (GR1) PE-Cy7 (RB6-8C5), CD117-APC (2B8), TCRβ APC-EF780 (H57-597) and B220 EF450 (RA3-6B2) (ThermoFisher). Apoptosis assays were performed by Annexin V/7-AAD staining according to the manufacturer's instructions (ThermoFisher). Cell cycle analysis was performed as described.[41]

Virus particle manufacture

Lentiviral and retroviral supernatants were prepared, and leukemic human and murine cells were infected with viral particles, as described.[39] Briefly, $4.5x10^6$ 293FT cells were plated overnight in 10mls DMEM with 10% FBS in 10cm dishes and transfected with 4μg lentiviral vector, 2μg pCMVR8.74 and 1μg of pMD2.G precomplexed with 21μg of PEI in serum free DMEM for 30 minutes at room temperature. Medium was changed the following day and 10^6 target cells sequentially transduced with 10ml of viral supernatant collected at 24hr and 48hr post transfection in the presence of 8μg/ml polybrene. Cells were selected using 3μg/ml puromycin for 24hrs prior to use.

shRNA cloning

2mM of forward and reverse complementary oligonucleotides were synthesised (Integrated DNA Technologies) and annealed in 1x CutSMART buffer by incubating at 95°C for 5 minutes and allowing to cool slowly to room temperature. 0.2mM of annealed oligonucleotides were then ligated into 50ng pLKO.1 predigested with EcoRI/AgeI restriction endonucleases at 16°C overnight and transformed into Stbl3 chemically competent cells.

Western blotting

Cells were harvested, washed twice with PBS and re-suspended in modified RIPA buffer (50mM Tris-HCl pH7.4, 100mM NaCl, 1% NP-40, 1% sodium deoxycholate, 0.1% Sarkosyl, 5mM $MgCl_2$, 3% glycerol) supplemented with 1x EDTA-free protease inhibitors (Roche, Basel, Switzerland), 0.5mM PMSF, 1mM DTT, 5mM sodium butyrate, 5mM sodium fluoride and 1:250 benzonase (Millipore, Burlington, MA). Re-suspended cells in lysis buffer were incubated for 50 minutes at room temperature on a rotating wheel and vortexed briefly every 10 minutes to facilitate cell lysis and protein extraction. Samples were then spun down at 20,817g for 30 minutes, at 4°C in a bench top centrifuge and supernatants (corresponding to the whole protein extracts) were collected and quantified by BCA assay (ThermoFisher). For protein subcellular fractionation a ThermoFisher kit (78840) was used, according to the manufacturer's instructions. Between 10 and 30μg of protein extract was mixed with NuPAGE LDS Sample buffer (ThermoFisher) and 100mM DTT and denatured for 5 minutes at 95°C before loading on an SDS-PAGE gel. Transfer of proteins to nitrocellulose membrane (Cytiva, Marlborough, MA) was carried out at 80V for 1 hour and 30 minutes at 4°C, or at 30V overnight at 4°C in Transfer buffer (Tris-Glycine) containing 10% methanol. Membranes were blocked in 5% milk in TBS/0.1% Tween for one hour at room temperature. Primary antibodies were diluted in 5% BSA dissolved in TBS/0.1% Tween and incubated with the membrane either overnight at 4°C, or for three hours at room temperature. After three washes with TBS/0.1% Tween (5 minutes each), membranes were incubated with the appropriate secondary antibodies diluted in 5% BSA in TBS/0.1% Tween for one hour at room temperature. After a further three washes, protein signals were detected by the Enhanced Chemo Luminescence (ECL) method (Bio-Rad, Hercules, CA) and images were acquired with the Chemidoc™ Touch Imaging System (Bio-Rad). Wherever possible western membranes were cut to facilitate probing for proteins of different molecular weights with different antibodies. Where protein sizes were similar (e.g. Figures 2E or 5J), membranes were stripped with Restore Western Blot Stripping Buffer (ThermoFisher) and reprobed with a different antibody. The following antibodies were used for western blot analysis at the indicated dilutions: anti-H3K9ac (ab4441, Abcam (Cambridge, UK), 1:10000), anti-H3K18ac (9675S, Cell Signaling Technology (Danvers, MA), 1:2000), anti-H3K27ac (ab4729, Abcam, 1:1000), anti-Total H3 (3638S, Cell Signaling Technology, 1:1000), anti-H4K5ac (8647S, Cell Signaling Technology, 1:1000), anti-Total H4 (2935S, Cell Signaling Technology, 1:1000), anti α-Tubulin (in house, 1:500), anti-EP300 (61401, Active Motif (Carlsbad, CA), 1:1000), anti-MYB (05-175, Merck Millipore (Burlington, MA), 1:1000 and ab45150, Abcam, 1:1000), anti-CEBPA (C15410225, Diagenode (Denville, NJ), 1:1000), anti-SPI1 (2258S, Cell Signaling Technology, 1:1000), anti-RUNX1 (ab23980, Abcam, 1:1000), anti-IRF4 (4964S, Cell Signaling Technology, 1:1000), anti-TCF3/E2A (12258S, Cell Signaling Technology, 1:1000), anti-CBP (ab253202, Abcam, 1:1000), anti-RFX5 (200-401-194, Rockland (Pottstown, PA), 1:1000), anti-FLI1 (ab133485, Abcam, 1:1000), anti-ETV6 (HPA000264, Atlas Antibodies (Bromma, SE, 1:500), anti-ELF1 (sc-133096, Santa Cruz Biotechnology (Dallas, TX), 1:100) and anti-Vinculin (V9131, Sigma Aldrich (St Louis, MO), 1:5000).

RNA sequencing

For experiments on THP1 AML cells, total RNA was extracted using the RNeasy Plus Mini Kit (Qiagen, Hilden, Germany), according to manufacturer's instructions. RNA quality was assessed using a Bioanalyzer 2100 (Agilent Technologies). Indexed poly-adenylated RNA libraries were prepared with an input of 500ng of total RNA using the SureSelect Strand-Specific RNA Library Prep System (G9691A, Agilent Technologies) or the NEB Next Ultra II Directional RNA Library Prep Kit (E7760, New England Biolabs) following ribosomal RNA depletion using the NEB Next rRNA Depletion Kit v2 (E7405, New England Biolabs) according to the manufacturer's instructions. Library quality was assessed using a Fragment Analyzer 5200 (Agilent Technologies). Libraries were quantified by qPCR using the KAPA Library Quantification Kit for Illumina (Roche). Sequencing was performed on a NovaSeq 6000 platform (Illumina) using NovaSeq SP consumables (2x100 cycles, paired-end, 30 million per sample). Reads were aligned to the human genome (GRCh38) and gene annotated with its corresponding GTF files (GENCODE GRCh38) using STAR version 2.4.2a with the settings–outFilterMultimapNmax 20,–outFilterType BySJout,–alignSJoverhangMin 8,–quantMode GeneCounts.[42] DESeq2 was used to perform differential gene expression analysis and calculate FPKM (fragments per kilobase of transcript per million mapped reads) values for each gene, counting only reads that mapped to exonic regions.[43]

For experiments on OPM-2 myeloma xenografts, tumour samples were collected into RNAlater (ThermoFisher) and incubated for 24h at 4°C before long term storage at -70°C. RNA was extracted from tumour samples using an RNeasy Plus Mini Kit (Qiagen), according to manufacturer's instructions. Nanodrop spectrophotometric QC was performed on extracted nucleic acids to determine concentration and purity. Bioanalyzer/Tapestation QC was performed on tumour RNA to assess integrity of the sample. Libraries were prepared with the KAPA RNA HyperPrep with RiboErase kit (Roche). Paired end 2x75 bp sequencing achieved an average of 50M reads per sample. Reads were aligned and FPKM calculated as above.

Single cell RNA sequencing (scRNA) library preparation and sequencing

Cryopreserved primary patient blood and BM samples pre- and post- treatment with CCS1477 were thawed and washed in 0.04% BSA/PBS. For single-cell RNA sequencing, libraries were prepared using the Chromium Single Cell 3' Reagent Kit using v3.1 chemistry in accordance with the manufacturer's (10x Genomics) protocol. Briefly, 25,000 cells from each sample were loaded on separate channels with a target output of 10000 single cells. Reverse transcription and library preparation were performed on a Veriti 96-well PCR (Applied Biosystems). The amplified cDNA and final libraries were evaluated on an Agilent Fragment Analyzer 5200 using the HS NGS Fragment kit. Libraries were pooled and sequenced on a NovaSeq6000 platform (Illumina) with a final loading concentration of 360pM using 28+10+10+90 cycles. Between 40,000 and 50,000 reads per cell were obtained.

10x Genomics scRNA sequencing processing and analysis

Cell Ranger (version 5.0.1) was used to align reads to human genome GRCh38-2020-A and for detecting cells using default parameters. Downstream high-level scRNAseq analysis was performed using the Seurat suite (version 4.1.1). Each sample was assessed separately and cells with high mitochondrial gene percentage (>0.10), low number of detected genes (<300) or a high UMI count, which potentially represents multiplets (>30,000), were removed. Counts were then normalised, scaled, and centered using sctransform methodology, as described.[44]

Highly variable genes were detected through dispersion of binned variance to mean expression ratios using the *FindVariableGenes* function of the Seurat package.[45] Principal component analysis was then performed on normalized expression values using top 3000 HVGs as input. To visualise and explore the data further, non-linear dimensionality reduction was performed using Uniform Manifold Approximation and Projection (UMAP) plots using the top 30 principal components of each dataset. Clustering of cells was performed using Seurat's shared-nearest neighbour (SNN) graph-based approach. Briefly, we first constructed and refined a K-nearest neighbour graph based on the Euclidean distance in PCA space using the *FindNeighbors* function, with the same 30 PCs as input, then applied the Louvain algorithm as the modularity optimization technique for grouping cells together into transcriptionally similar "communities", as described.[46]

Cluster specific markers were calculated using the *FindMarkers* function from the Seurat package with the following parameters: min.pct = 0.25, logfc.threshold = 0.25. This function uses the nonparametric Wilcoxon test on the log transformed, normalized UMIs to compare expression level. Cluster cell identities were then inferred by assessing canonical gene expression patterns in each cluster and by assessing cluster specific genes. Cell signature gene sets were collated by curating known canonical cell markers selected from multiple hematopoiesis datasets. To confirm our output, we used SingleR for automatic cluster annotation using the single-cell datasets described.[47]

For the integration of single-cell datasets, we used a combination of the Scanpy and Scanorama packages, which use Mutual Nearest Neighbour method (MNN) for sample alignment, then visualised them through dimensionality reduction.[48] Cluster annotation was repeated using the same method described above. For the assessment of transcriptional changes in the blasts across the different timepoints, we aggregated the raw counts of this cell population in each sample to obtain pseudo-bulk datasets. We then normalised the datasets using the normalisation framework provided by the *DESeq2* package.

Quantitative PCR analysis

Reverse transcription of total RNA was carried out with the High-Capacity cDNA Reverse Transcription kit (Applied Biosystems, Waltham, MA), according to the manufacturer's instructions. Real time (RT) PCR was performed in triplicate, in a 10μl final reaction volume composed of 5μl TaqMan Fast Universal PCR Master Mix (Applied Biosystems), 25ng of cDNA, and 0.5μl of TaqMan premixed primers with probes (Hs00358836_m1 for *KLF4*, Hs00269972_s1 for *CEBPA*, Hs00153408_m1 for *MYC*, Hs00920556_m1 for *MYB*, Hs00180031_m1 for *IRF4*, Hs02786624_g1 or Hs01922876_u1 for *GAPDH*, and Hs02598545_g1 for *H3F3A*). Quantitative PCR amplifications were carried out in a QuantStudio™ 5 instrument (Applied Biosystems), using the following protocol: 1) 95°C for 20 seconds, 2) 40 cycles at 95°C for 1 second and 60°C for 20 seconds. To assess enhancer RNAs (eRNA), RT-PCR was performed by mixing 45ng of cDNA (using the High-Capacity cDNA Reverse Transcription kit) with 5μl of 2X SYBR green Master Mix (ThermoFisher, 4309155) and 0.5μM of each primer mix in a final reaction volume of 10μl. Quantitative PCR amplifications were performed in the QuantStudio™ 5 instrument (Applied Biosystems, A28140), using the following protocol: 1) 50°C for 2 minutes, 2) 95°C for 10 minutes, 3) 40 cycles at 95°C for 15 seconds and 60°C for 1 minute. Primers were designed either on the H3K27ac or the phosphoS2 Pol II peak (at intronic or intergenic regions) closest to the EP300 binding region at the selected enhancers. The primer sequences used are shown in Table S4.

Chromatin immunoprecipitation (ChIP) and next generation sequencing

For chromatin immunoprecipitation experiments with THP1 AML and OPM-2 myeloma cells, $70x10^6$ cells were treated for 1, 2, 6 or 48 h with CCS1477 (100nM and 1000nM), or DMSO vehicle. Cells were cross-linked using 1% formaldehyde (Sigma Aldrich) in PBS for 10 minutes (for H3K27ac, RNA-Pol II, phosphoS2 RNA-Pol II, phosphoS5 RNA-Pol II and CEBPA), or double cross-linked (for EP300, MYB, IRF4, CBP, TCF3/E2A and RUNX1) with ChIP cross-link Gold (Diagenode) for 30 minutes in PBS containing 1mM $MgCl_2$ and then with 1% formaldehyde for 10 minutes. The reaction was stopped by addition of 0.125M glycine for 5 mins. Cell pellets were then washed twice with cold PBS containing protease inhibitors (Complete EDTA-free tablets, Roche). ChIP was performed as described.[49] Briefly, nuclear lysates were sonicated by using a Bioruptor Pico for 8 and 16 cycles (30 seconds ON, 30 seconds OFF settings) for THP1 and OPM-2 cells, respectively. Chromatin Immunoprecipitation was carried out overnight at 20 rpm, 4°C in a rotating wheel with 180μl Dynabeads Protein G (10004D, Invitrogen) previously conjugated with 15μg antibody.

The antibodies used for ChIPseq analysis were: anti-EP300 (61401 from Active Motif and MCA6390 from Bio-Rad), anti-H3K27ac (ab4729 from Abcam), anti-CEBPA (C15410225 from Diagenode), anti-MYB (ab45150 from Abcam), anti-IRF4 (4964S from Cell Signalling Technology), anti-CBP (ab253202 from Abcam), anti-TCF3/E2A (12258S from Cell Signalling Technology), anti-RUNX1 (ab23980 from Abcam), anti-Total RNA-Pol II (ab26721 from Abcam), anti-phospho S2 RNA-Pol II (ab5095 from Abcam) and anti-phospho S5 RNA-Pol II (ab5408 from Abcam).

Beads were then washed six times with RIPA buffer (50mM HEPES pH7.5, 1mM EDTA, 0.7% Na deoxycholate, 1% NP-40, 0.5M LiCl) and once with TE buffer (10mM Tris pH8.0, 1mM EDTA). Next, chromatin IP-bound fractions were extracted and de-crosslinked with Odom elution buffer (50mM TrisHCl pH8.0, 10mM EDTA, 1% SDS) and incubated in a thermomixer at 65°C and 900 rpm

overnight. The day after, RNaseA (0.2mg/ml) and proteinase K (0.2 mg/ml) were added to remove any RNA and protein from the samples. Finally, DNA was extracted using phenol:chloroform:isoamyl alcohol extraction and precipitated with ethanol: two volumes of ice-cold 100% ethanol, glycogen (0.075μg/μl) and 200mM NaCl were added to each sample. Samples were then incubated overnight at −80°C. Pellets were washed with 70% ethanol and resuspended in 30μl 10mM TrisHCl pH8.0.

ChIP DNA samples were prepared for sequencing using the NEB Next UltraII kit (New England Biolabs) starting from 1-5ng of ChIP DNA, according to the manufacturer's instructions. Libraries were size selected with AMPure XP beads (Beckman Coulter, USA) for 200-800 base pair size range and quantified by qPCR using a KAPA Library Quantification Kit for Illumina (Roche). Sequencing was performed on a NovaSeq 6000 platform (Illumina) using NovaSeq SP consumables (2x100 cycles or 2x150 cycles, paired-end, 50-100 million reads per sample). Reads were aligned to the human genome (hg38) using BWA-MEM v0.7.15. Reads were further filtered using Samtools v0.1.9 and Bedtools v2.25.0 to keep only reads that mapped to standard chromosomes and to remove reads mapped to blacklisted regions defined by ENCODE (http://mitra.stanford.edu/kundaje). MACS2 (Model-based Analysis of ChIPseq, version 2.1.0) software was used to call peaks.[50] A cutoff of 0.01 False Discovery Rate (FDR) was used as a threshold and five duplicates were allowed (callpeak –t ChIP.bam -f BAMPE -c input.bam –keep-dup 5 -g hs -B -q 0.01). Annotation of peaks was performed with Homer version 4.10.[51] The genomic coordinates of peak apices were set at the centers of 100 bp regions to create BED files using the package GenomicRanges (version1.30.1) (R/Bioconductor).[52] Then they were used for evaluating the intersection of peaks between different ChIPseq experiments with the BEDtools package (version 2.25.0). All high throughput sequencing data files are available at the Gene Expression Omnibus: GSE207357.

ChIP-qPCR

ChIP-qPCR was performed as follows: 2.5μl ChIP DNA (prepared as described in the paragraph "Chromatin immunoprecipitation (ChIP) and next generation sequencing") and input samples (all diluted 1:5) was mixed with 5 μl of 2X SYBR green Master Mix (Applied Biosystems, 4309155) and 0.5 μM of each primer mix in a final reaction volume of 10μl. Quantitative PCR amplifications were performed in the QuantStudio™ 5 instrument (Applied Biosystems, A28140), using the following protocol: 1) 50°C for 2 minutes, 2) 95°C for 10 minutes, 3) 40 cycles at 95°C for 15 seconds and 60°C for 1 minute. The primer sequences used are shown in Table S4.

ATAC sequencing

THP1 AML and OPM-2 myeloma cells were treated with DMSO or 100nM CCS1477 for 6h and 48h. Cells were washed once with ice-cold PBS and Assay for Transposase Accessible Chromatin (ATACseq[53]) was performed using 50,000 viable cells. Cell pellets were re-suspended in 50μL ice-cold lysis buffer (10mM Tris-HCl pH7.4, 10mM NaCl, 3mM $MgCl_2$, 0.1% IGEPAL CA-630) and nuclei were pelleted by centrifugation for 10 minutes at 500g. Supernatant was discarded and nuclei were suspended in 25μL reaction buffer containing 2μL Tn5 transposase (Diagenode, C01070012) and 12.5μl Tagmentation buffer (Diagenode, C01019043). The reaction was incubated for 45 minutes at 37°C and 300rpm and purified using a MinElute PCR Purification Kit (QIAGEN). Library fragments were amplified using 2x NEB Next High-Fidelity PCR master mix and 1.25μM of custom PCR primers and conditions.[53] The PCR reaction was monitored to reduce GC and size bias by amplifying the full libraries for five cycles and taking an aliquot to run for 20 cycles using the same PCR cocktail and 0.6x SYBR Green (ThermoFisher). The remaining 45μl reaction was amplified for additional cycles as determined by qPCR. Libraries were finally purified using a MinElute PCR Purification Kit. Libraries were size selected with AMPure beads for 200-800 base pair size range and quantified by qPCR using a Kapa Library Quantification Kit. ATACseq data were generated using the NovaSeq platform from Illumina with a 2x100bp output.

Sequencing reads were quality checked using FASTQC v0.11.3.[54] Any adaptor sequences present in the data were removed using Cutadapt.[55] The cleaned and trimmed FASTQ files were mapped to the hg38 reference assembly using BWA-MEM v0.7.15[56] and processed using Samtools v0.1.9.[57] The data were cleaned for duplicates, low mapping quality reads (i.e., MAPQ < 30), non-uniquely mapped reads, not properly paired reads and reads mapped to non-conventional chromosomes and mitochondrial DNA.

Bromodomain assays

Bromoscanning was performed by DiscoverX Corporation (Fremont, CA) using methodology adapted from.[58] BROMO*scan* employs a proprietary ligand binding site-directed competition assay to quantitatively measure interactions between test compounds and bromodomains. As an overview, assay components (cell-expressed bromodomain labeled with DNA tag for qPCR readout, a known control bromodomain ligand immobilized on a solid support, and CCS1477 test compound or control) were assembled and equilibrated, and then the solid support was washed to remove unbound bromodomains. Bromodomains captured on the solid support were quantified by qPCR and captured bromodomain levels in test and control conditions were then compared.

In detail, T7 phage strains displaying bromodomains were grown in parallel in 24-well blocks in an *E. coli* host derived from the BL21 strain. *E. coli* were grown to log-phase and infected with T7 phage from a frozen stock (multiplicity of infection = 0.4) and incubated with shaking at 32°C until lysis (90-150 minutes). The lysates were centrifuged (5,000 x g) and filtered (0.2μm) to remove cell debris. Streptavidin-coated magnetic beads were treated with biotinylated small molecule or acetylated peptide ligands for 30 minutes at room temperature to generate affinity resins for bromodomain assays. The liganded beads were blocked with excess biotin and washed with blocking buffer (SeaBlock (Pierce), 1 % BSA, 0.05 % Tween 20, 1 mM DTT) to remove unbound ligand and to reduce non-specific phage binding. Binding reactions were assembled by combining bromodomains, liganded affinity beads, and test compounds in 1x binding buffer (16 % SeaBlock, 0.32x PBS, 0.02%BSA, 0.04 % Tween 20, 0.004% Sodium azide, 7.9 mM DTT). Test compounds were prepared as 1000X stocks in 100% DMSO and subsequently diluted 1:25 in monoethylene glycol (MEG). The

compounds were then diluted directly into the assays such that the final concentrations of DMSO and MEG were 0.1% and 2.4%, respectively. All reactions were performed in polypropylene 384-well plates in a final volume of 0.02 ml. The assay plates were incubated at room temperature with shaking for 1 hour and the affinity beads were washed with wash buffer (1x PBS, 0.05% Tween 20). The beads were then re-suspended in elution buffer (1x PBS, 0.05% Tween 20, 2 μM non-biotinylated affinity ligand) and incubated at room temperature with shaking for 30 minutes. The bromodomain concentration in the eluates was measured by qPCR.

QUANTIFICATION AND STATISTICAL ANALYSIS

Gene set enrichment analysis

Pre-ranked gene set enrichment analysis was performed with GSEA v2.0.14 software from https://www.broadinstitute.org/gsea.[59] Genes were rank ordered according to $\log_2$ fold change in expression.

Statistics

Statistical analyses were performed using Microsoft Excel 2016 or StatsDirect software (v.1.9.7). Details of the statistical tests used for each analysis shown may be found in the figure legends.